agronomy

MDPI

Article

Physiological Response to Salinity in Novel M-Series Grapevine Rootstocks: A Comparison with Commercial Standards

Xavier Rius-Garcia [1,2], María Videgain-Marco [1,3], José Casanova-Gascón [1,3], Luis Acuña-Rello [4] and Pablo Martín-Ramos [4,*]

[1] Department of Agricultural and Environmental Sciences, Higher Polytechnic School of Huesca, University of Zaragoza, Ctra. Cuarte s/n, 22071 Huesca, Spain; xrius@agromillora.com (X.R.-G.); mvidegain@unizar.es (M.V.-M.); jcasan@unizar.es (J.C.-G.)
[2] Agromillora Group, Plaça Manel Raventós 3-5, St. Sadurní d'Anoia, 08770 Barcelona, Spain
[3] AgriFood Institute of Aragón (IA2–CITA–University of Zaragoza), Ctra. Cuarte s/n, 22071 Huesca, Spain
[4] Department of Agricultural and Forestry Engineering, ETSIIAA, University of Valladolid, Avda. Madrid 44, 34004 Palencia, Spain; luis.acuna@uva.es
* Correspondence: pmr@uva.es

Abstract: Rising soil salinity poses significant challenges to Mediterranean viticulture. While some rootstocks effectively reduce salt accumulation in grafted scions, the mechanisms and performance of novel rootstocks remain largely unexplored. This study compared two novel M-series rootstocks (M2, M4) with established commercial rootstocks (1103 Paulsen, R110) to evaluate their physiological responses and salt tolerance under irrigation with varying salinity levels (0, 25, 50, and 75 mM NaCl) over 5 months. Growth parameters, photosynthetic efficiency, chlorophyll content (SPAD), ion homeostasis, and visual symptoms were monitored. Results revealed genotype-specific strategies: 1103 Paulsen exhibited robust photosynthetic efficiency and ion exclusion, maintaining growth and chlorophyll stability; M2 demonstrated superior biomass retention and moderate ion compartmentalization but showed reduced photosynthetic performance at higher salinity levels; R110 displayed effective ion management at moderate salinity but experienced significant growth reduction under severe stress; and M4 was the most sensitive, with severe reductions in growth and ion homeostasis. Organ-specific responses highlighted roots acting as primary ion reservoirs, particularly for sodium and calcium; leaves exhibited high potassium and chloride concentrations, critical for photosynthesis but prone to ionic imbalance under stress; and stems and wood played a buffering role, compartmentalizing excess sodium and minimizing damage to photosynthetic tissues. The reported findings provide valuable insights for rootstock selection and breeding programs, particularly for regions facing increasing soil and water salinization challenges.

Keywords: *Vitis vinifera*; abiotic stress; chlorophyll fluorescence; genetic variability; ion homeostasis; M2; M4; photosynthetic efficiency; rootstock selection; salt tolerance

Academic Editor: Rosa Porcel

Received: 26 December 2024
Revised: 12 February 2025
Accepted: 13 February 2025
Published: 15 February 2025

Citation: Rius-Garcia, X.; Videgain-Marco, M.; Casanova-Gascón, J.; Acuña-Rello, L.; Martín-Ramos, P. Physiological Response to Salinity in Novel M-Series Grapevine Rootstocks: A Comparison with Commercial Standards. *Agronomy* **2025**, *15*, 473. https://doi.org/10.3390/agronomy15020473

1. Introduction

Vitis vinifera L., the common grapevine, is a keystone species within the Vitaceae family, cultivated primarily for wine, table grapes, and raisins [1]. The Mediterranean region represents 39% of the total vineyard surface (7.3 million hectares), with Spain, France, Italy, and Turkey being major producers [2].

Mediterranean viticulture faces two significant environmental challenges: recurring drought and rising soil salinity [3–5]. Climate projections suggest these pressures will

intensify, threatening the sustainability of traditional wine-growing regions [6]. Grapevines' moderate salt tolerance makes them particularly vulnerable to soil salinization, which can compromise vine productivity, alter berry composition, and reduce wine quality [7,8]. In fact, many authors are actively investigating different approaches to address these salinity challenges, from rootstock-based solutions [9] to soil amendments [10,11]. Recent findings on salt-excluder rootstocks have shown promising results in improving physiological responses under salinity stress [9], while complementary research explores soil management strategies using zeolite applications to enhance vine performance under challenging conditions [10,11].

Salinity stress severely affects plant growth, disrupting shoot development, reducing leaf size, altering gas exchange, and impairing carbon storage, ultimately leading to yield reductions [9]. It accelerates leaf senescence, damages cellular membranes, and decreases photosynthetic pigment levels, compromising overall plant health and potentially causing mortality [9]. The stress operates through osmotic and ionic components: the former limits water uptake and reduces cell expansion, while the latter involves toxic ion accumulation, particularly Na^+ and Cl^-, in leaves [12]. Plants counteract salinity stress through mechanisms such as root exclusion of harmful ions and compartmentalization into vacuoles or woody tissues, thus protecting photosynthetic tissues and enabling growth under saline conditions [13].

Specific grapevine rootstocks, such as 1103 Paulsen, Ramsey, and 140 Ruggeri, can significantly reduce salt accumulation in grafted *V. vinifera* scions [13,14]. These rootstocks are widely used to combat salinity; however, the exact mechanisms of their enhanced tolerance remain unclear [15]. A rootstock's capacity to impart salt tolerance is influenced by factors beyond nutrient selectivity, including the ability to store Na^+ ions within the vacuoles of root pericycle cells [16] and the capacity of stems to compartmentalize Cl^- and Na^+ [17], with more vigorous rootstocks often demonstrating higher salinity tolerance [18].

Despite efforts to breed salt-tolerant rootstocks, the limited number in common use remains a constraint in viticulture, restricting the ability to respond to evolving biotic and abiotic stresses [19,20]. Public and private research programs seek to address this by developing new stress-resistant rootstocks [21]. In the case of the University of Milan, among their released "M" series genotypes [22,23], the M2 and M4 rootstocks intend to improve grapevine resilience to salinity and drought, making them valuable for viticulture in challenging environments [24,25].

This study aims to evaluate the physiological mechanisms underlying salinity tolerance in novel M-series rootstocks (M2, M4) compared to established commercial standards (1103 Paulsen, R110). We hypothesize the following: (1) that the M-series rootstocks will demonstrate enhanced salt tolerance through more effective Na^+ and Cl^- exclusion mechanisms; (2) that this enhanced ion regulation will result in better maintenance of physiological functions under salt stress; and (3) that genotype-specific responses will vary across different salinity thresholds. To test these hypotheses, we evaluated differences in ion compartmentalization and transport through mineral content analysis, osmotic adjustment capacity through physiological indicators, photosynthetic efficiency through chlorophyll fluorescence, and growth parameters and visual damage assessment across four salinity levels (0–75 mM NaCl). The findings will provide evidence-based guidance for rootstock selection in salinity-affected vineyards and contribute to the advancement of breeding programs targeting salt tolerance in Mediterranean viticulture.

2. Materials and Methods

2.1. Location and Experimental Design

The experiment was conducted in a polyethylene greenhouse at the Universidad de Zaragoza, Spain (42°07′12.78″ N, 0°26′49.04″ O). In June 2022, uniform 12-month-old rootstocks of four grapevine genotypes (1103 Paulsen, 110 Ritchter, M2, M4) were obtained from Vivai Cooperativi Rauscedo (Rauscedo, PN, Italy) and transplanted into 4.5 L pots with quartziferous sand (0.05–2.00 mm), after root cleaning with deionized water. Following a 7-month cultivation period and January pruning, the experiment ran from June to November 2023, initiating when shoots reached 50 cm in height. Greenhouse conditions were maintained at 18–33 °C with 55–85% day/night relative humidity, regulated by automated shading (activated > 27 °C) and ventilation systems.

The study employed a completely randomized block design with four salinity treatments (0, 25, 50, and 75 mM NaCl) per rootstock genotype (n = 4 plants per treatment, total N = 64). These concentrations were selected to represent both current and projected irrigation quality challenges: 25 and 50 mM NaCl reflect typical ranges in brackish irrigation water, while 75 mM NaCl was included to evaluate responses under extreme stress conditions and identify genotype-specific tolerance thresholds. This range aligns with previous grapevine salinity studies (e.g., Nikolaou et al. [1], using 0–100 mM NaCl gradients) while encompassing projected salinity increases under climate change scenarios.

2.2. Irrigation Management

The nutrient solution used in this experiment was a 1/4 strength Hoagland solution [26], prepared by diluting the standard formula with local fresh water, which had an initial electrical conductivity (EC) of 0.8 dS m^{-1}. The four rootstock genotypes were subjected to four salinity treatments (0, 25, 50, and 75 mM NaCl) over five months. Salinity levels were increased by 25 mM NaCl per week until the target concentrations were achieved on 1 June 2023.

Irrigation frequency and duration were adjusted according to weather conditions, with four-minute sessions occurring one to three times daily. Each pot was irrigated through two drippers delivering 1.3 L h^{-1} (Click Tip HD, Naandanjain, Jalgaon, India). Saline solutions were injected into the irrigation system using a MixRite E-300 volumetric pump (Tefen Flow and Dosing Technologies LTD, Kibbutz Farod, Israel). An Agronic 5500 irrigation controller (Sistemes Electrònics PROGRÉS, Barcelona, Spain) regulated irrigation events to ensure precise delivery of the saline treatments.

The irrigation water's electrical conductivity (EC_{iw}) and sodium adsorption ratio (SAR_{iw}) levels were 0.8, 3.0, 6.0, and 9.0 dS m^{-1} and 2, 30, 60, and 90, respectively, with pH values between 7.2 and 7.4. During the experiment, drainage water from each treatment was collected weekly for analysis of leached solutes. Electrical conductivity measurements in the leaching solution were carried out using a Hanna Instruments-HI 9033 conductivity meter (Woonsocket, RI, USA). The values measured for 0, 25, 50, and 75 mM NaCl concentrations were 0.8, 3.2, 6.1, and 9.2 dS m^{-1}, respectively. This confirmed that maintaining a 20–30% leaching fraction during irrigation ensured a consistent salinity level in the pots throughout the experiment [27].

2.3. Plant Material Analysis

Every 15 days, shoot length, trunk diameter at 10 cm (using a digital ABS caliper, Hoffman Group, Munich, Germany), and visual damage of four plants per treatment were monitored. Salt-induced leaf necrosis was assessed visually on a scale from 0 to 5, according to the percentage of the total leaf area affected (0: no symptoms; 1: 20%; 2: 40%; 3: 60%; 4: 80%; 5: >80% of the plant canopy).

At the end of the experiment, plants were removed from the substrate and partitioned into roots, wood, stem, and leaves. Aerial plant parts were washed with distilled water, while roots were washed with deionized water to remove residual salts. Fresh masses of all plant parts were recorded, and dry weights were determined after oven-drying at 70 °C for 24 h.

The dried plant materials were ground into particles smaller than 2 mm using an electrical grain grinder (CGoldenwall model HC400, Wuxi, Jiangsu, China). The resulting material was analyzed through a combination of wet chemistry methods and a Niton XL3t GOLDD+ portable X-ray fluorescence (pXRF) spectrometer (Thermo Scientific, Waltham, MA, USA). The <2 mm particle size was chosen to simulate the physical conditions of processed soil samples that can be measured by a pXRF probe, following the protocols established by Sapkota et al. [28], Antonangelo and Zhang [29], and Towett et al. [30]. pXRF measurements were performed using the "Soil mode" for Ca^{2+} and K^{+} analysis and the "Mining mode" for Cl^{-} determination [31,32]. To ensure accuracy, pXRF measurements for cations were calibrated against atomic absorption spectrometry (SpectrAA 10 apparatus; Varian, Palo Alto, CA, USA), as a reference method, while ionic chromatography analysis—outsourced to Eurofins Scientific (Sidamon, Lleida, Spain)—was chosen as a reference for Cl^{-} calibration.

For Na^{+} determination, the dried and ground plant material (0.5 g per sample) was predigested for 1 h with 10 mL of trace metal-grade HNO_3. The digests were then heated to 115 °C for 2 h, diluted to a final volume of 50 mL with deionized water [33], and analyzed using atomic absorption spectrometry, following the procedure described by Kalra [34]. All values reported are the averages of four repeated measurements per sample.

2.4. Physiological Parameters

Physiological parameters including chlorophyll fluorescence, stomatal conductance, and leaf chlorophyll content (SPAD) were assessed at biweekly intervals. Chlorophyll fluorescence parameters were recorded using a portable Handy PEA fluorimeter (Hansatech Instruments Ltd., Norfolk, UK). Parameters including initial (F_0), maximum (F_m), and variable ($F_v = F_m - F_0$) fluorescence, and maximum quantum yield of photosystem II (PSII) (F_v/F_m) in dark-adapted leaves, as well as steady-state (F_s) and maximum (F'_m) fluorescence in light-adapted leaves were recorded. The fluorimeter-derived parameters were categorized into three groups: overall efficiency of PSII, energy and electron transport, and energy dissipation and damage [35–37].

Stomatal conductance (gs, mmol H_2O m^{-2} s^{-1}) was measured using a portable porometer (SC-1 model, Meter Group, Pullman, WA, USA). Measurements were made on two well-exposed and fully expanded leaves from the median part of the shoot from four plants per treatment and rootstock genotype, between 9:00 a.m. and 11:00 a.m.

Total leaf chlorophyll content was determined using a portable SPAD-502Plus chlorophyll meter (Konica Minolta, Osaka, Japan), allowing rapid, non-destructive measurements [38]. SPAD values were obtained from fully expanded functional leaves, with the operator shielding the meter from direct sunlight during each measurement. Fifteen leaves were randomly selected from each rootstock genotype and treatment, and their values were averaged to obtain a single SPAD value.

2.5. Statistical Analysis

Statistical analyses were performed using R software (version 4.4.1:2024) [39] and IBM SPSS v. 26 (IBM, Armonk, NY, USA). A complete 3-factor factorial design (rootstock genotype, treatment, and organ) was established, with 4 levels each and 4 repetitions, totaling $4^3 \times 4 = 256$ trials. Analyzing the samples from each trial allowed the values of

the target variables (Ca^{2+}, K^+, Cl^-, Na^+, fresh weight, and dry weight) to be obtained. Along with these variables, the behavior of the most important relationships between them was also analyzed: Ca^{2+}/Na^+ and K^+/Na^+. The normality of the data was checked for all populations using the Kolmogorov–Smirnov normality test with Lilliefors correction [40] or the Shapiro–Wilk test [41], depending on the amount of data in the groups, and the Q–Q normal probability plot. This test was virtually always unfulfilled. The requirement of homoscedasticity was contrasted by the Levene test [42], being defaulted in many cases, so the usual comparative analysis based on linear statistics, ANOVA, could not be used. To solve this impediment, two statistical techniques were used: the Kruskal–Wallis test [43], when the distribution was not normal but the groups were homoscedastic; and Welch's heteroscedastic F test with trimmed means and Winsorized variances when neither normality nor homoscedasticity could be assumed. This latter robust procedure tests the equality of means by substituting trimmed means and Winsorized variances for the usual means and variances [44,45]. Bootstrapping methods were used to establish robust confidence intervals for location [46] and robust homogenous groups.

Natural cubic spline models [47–49] were chosen as response models, and their performance was analyzed for each target variable (shoot length, trunk diameter, SPAD, and stomatal conductance) through residual analysis, with the correlation coefficient (R^2 value) [50], the Akaike information criterion (AIC) [51], and the Bayesian information criterion (BIC) [52,53]. These values, together with the likelihood-ratio and Wald's tests, made it possible to establish the model's goodness of fit.

For the reduction and analysis of multivariate data, a principal component analysis (PCA) was performed based on the correlation matrix calculated using Spearman's coefficient, which is appropriate for non-parametric variables. Subsequently, a Varimax rotation was applied to facilitate the interpretation of the factors identified. The selection of the number of components was based on the criterion of eigenvalues greater than 1 and the cumulative percentage of variance explained.

3. Results

3.1. Growth Responses Under Salinity Stress

3.1.1. Fresh and Dry Weight

Analysis of growth parameters revealed distinct salinity responses among rootstock genotypes. In the absence of salinity stress, 1103 Paulsen demonstrated superior biomass accumulation in fresh weight (91.04 ± 4.23 g) compared to M4 and R110 ($p < 0.05$), and in dry weight (38.59 ± 1.82 g) compared to M4, as shown in Tables S1 and S3. With increasing salinity, genotype-specific patterns emerged (Figures S1 and S3): at 25 mM NaCl, 1103 Paulsen was the only genotype that experienced a significant decrease in fresh weight compared to the control ($p < 0.05$). Under 50 mM NaCl, all genotypes showed significant biomass reductions in terms of dry weight ($p < 0.05$), though M2 maintained significantly higher fresh weight (48.41 ± 2.31 g) compared to other genotypes ($p < 0.05$). The most severe impact was observed in M4, which showed consistent sensitivity across all stress levels, experiencing reductions of 69.0% in fresh weight and 65.4% in dry weight under 75 mM NaCl, with significant differences compared to M2 and 1103 Paulsen in terms of fresh and dry weight, respectively ($p < 0.05$). For comparison, M2 experienced reductions of 47.3% and 50.4% in fresh and dry weights, respectively; 1103 Paulsen displayed reductions of 63.2% in fresh weight and 58.8% in dry weight; and R110 presented reductions of 59.7% in fresh weight and 53.0% in dry weight. Hence, the ranking in terms of biomass maintenance was as follows: M2 > R110 > 1103 Paulsen > M4.

Organ-specific analyses also revealed distinct response patterns to salinity stress (Tables S2 and S4). Leaf tissue exhibited the greatest sensitivity to salinity stress, experi-

encing substantial reductions in both fresh (90.6%) and dry weight (79.2%) under severe stress conditions. In contrast, stems exhibited remarkable tolerance, showing moderate reductions (44.2% in fresh weight and 50.1% in dry weight) while maintaining high absolute weights across treatments. As shown in Figures S2 and S4, root tissue displayed intermediate sensitivity (51.7% fresh weight and 59.5% dry weight reduction), while wood tissue showed unique characteristics, with the smallest dry weight reduction (36.1%) but high variability across treatments.

3.1.2. Shoot Length

Differences in shoot length as a function of rootstock genotype and treatment are summarized in Table S5. Under control conditions (Figure 1a), M2 exhibited the most vigorous growth, reaching approximately 430 cm, followed by R110 at 400 cm, 1103 Paulsen at 350 cm, and M4 at 300 cm. All rootstock genotypes displayed steep growth curves, indicating rapid and sustained development. At 25 mM NaCl (Figure 1b), overall growth decreased, with M2 maintaining the highest shoot length at 340 cm, while R110 and 1103 Paulsen reached 270–290 cm, and M4 approximately 250 cm. The 50 mM NaCl treatment (Figure 1c) further reduced growth, with M2 reaching 280 cm, while the other rootstock genotypes clustered between 200 and 230 cm. Growth curves at this salinity level showed a more gradual increase, suggesting slower growth rates. At 75 mM NaCl (Figure 1d), M2 reached 230–240 cm, 1103 Paulsen and M4 reached 190 cm, and R110 showed the lowest growth (160 cm). The flatter growth curves at this salinity level indicated a substantial impact on shoot elongation rates across all rootstock genotypes, with M2 consistently demonstrating the highest salt tolerance in terms of shoot growth.

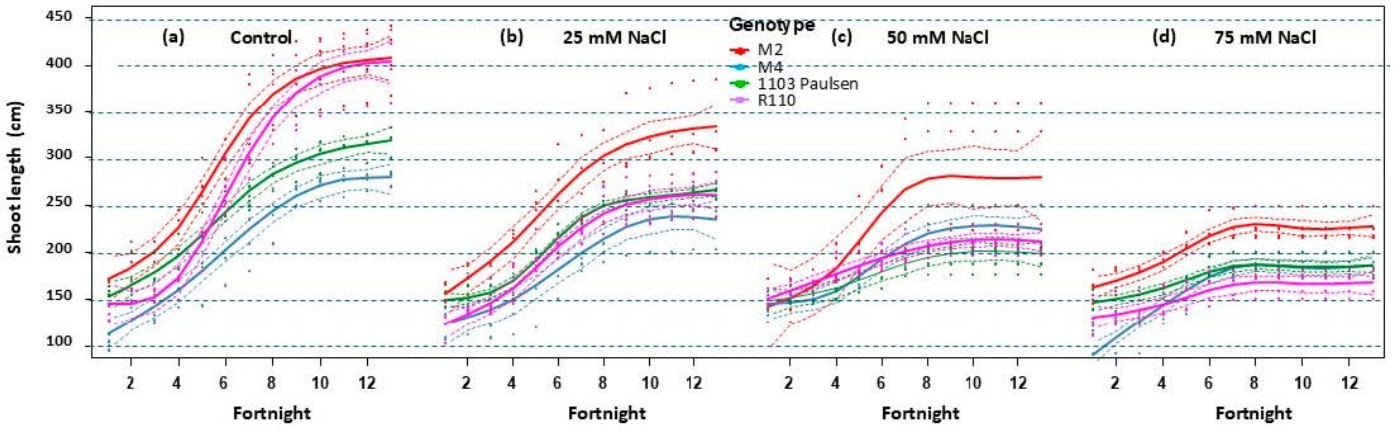

Figure 1. Spline representation of shoot lengths for each treatment as a function of rootstock genotype (M2, M4, 1103 Paulsen, and R110) and date (spanning 13 fortnights). For each genotype, the central line depicts the fitted spline curve, providing an approximation of shoot length growth trends, while the dotted lines above and below indicate the 95% confidence intervals.

If shoot length is plotted as a function of rootstock genotype (Figure S5), it can be observed in a clearer manner that R110 exhibited the most pronounced response to salinity stress (60% reduction), followed by M2 (43.2% reduction), 1103 Paulsen (40.6% reduction), and M4 (32.1% reduction).

3.1.3. Trunk Diameter

Spline data illustrating the differences in trunk diameter among rootstock genotypes and treatments is presented in Table S6. Under control conditions (Figure 2a), M2 attained the largest trunk diameter (7.8 mm by fortnight 10), followed by 1103 Paulsen (7.6 mm), R110 (6.5 mm), and M4 (6.0 mm). At 25 mM NaCl (Figure 2b), overall growth decreased, with M2 maintaining the largest diameter (8.0 mm), while R110 and 1103 Paulsen reached

7.0–7.5 mm, and M4 about 6.0 mm. The 50 mM NaCl treatment (Figure 2c) further reduced growth, with M2 reaching 7.5 mm and other rootstock genotypes clustering between 5.5 and 7 mm. At 75 mM NaCl (Figure 2d), M2 and R110 achieved similar diameters of 6.0–6.5 mm, 1103 Paulsen reached 5.5 mm, and M4 exhibited the smallest diameter (5.0 mm).

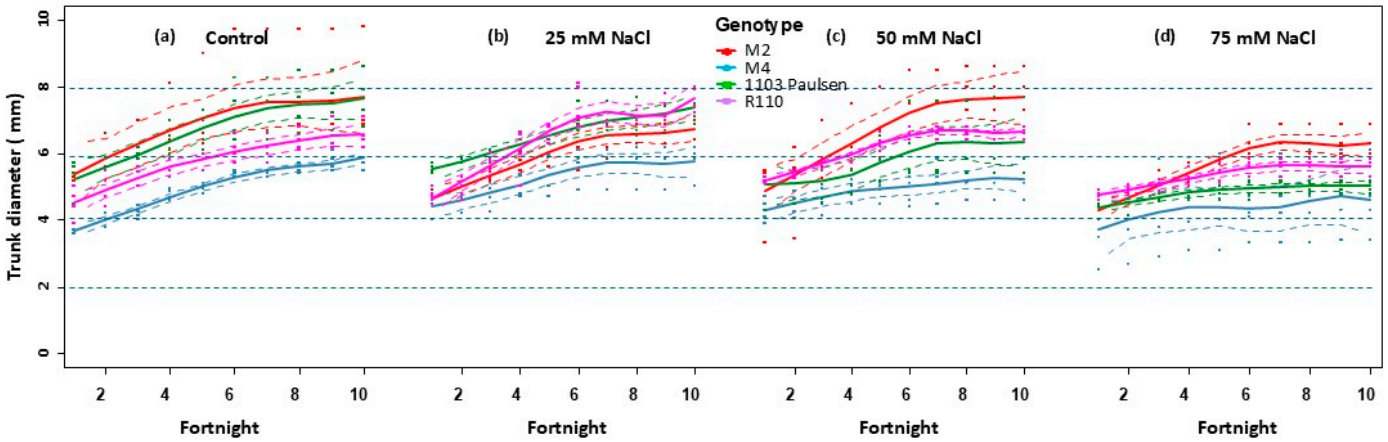

Figure 2. Spline representation of trunk diameters for each treatment as a function of rootstock genotype (M2, M4, 1103 Paulsen, and R110) and date (spanning 13 fortnights). For each genotype, the central line depicts the fitted spline curve, providing an approximation of trunk diameter growth trends, while the dotted lines above and below indicate the 95% confidence intervals.

When the final diameters at 75 mM NaCl were compared with those under control conditions as a function of rootstock genotype (Figure S6), 1103 Paulsen exhibited the most pronounced reduction in response to salinity treatment (34.6%), followed by M4 (20.0%), M2 (19.3%), and R110 (8.0%).

3.2. Physiological Adaptations to Salinity Stress

3.2.1. Fluorimetry

Statistical data on fluorimetry across treatments and rootstock genotypes are summarized in Table S7. The electron flux assessment (Figure 3a) showed that, under control conditions, M2 exhibited enhanced electron transport beyond QA (i.e., the turnover number of primary quinone electron acceptors) per reaction center (REo/RC) values compared to other genotypes. With increasing salinity, the maximum quantum yield (φ(Po)) and electron transport probability (ψ(Eo)) progressively decreased, particularly in M2 and M4 at 75 mM NaCl. 1103 Paulsen maintained stable electron transport characteristics across treatments, while M2 displayed pronounced sensitivity, with substantial decreases in electron transport efficiency. R110 showed intermediate responses, maintaining moderate electron transport capacity under mild stress but declining at higher salinity levels.

The energy dissipation analysis (Figure 3b) revealed that 1103 Paulsen exhibited the highest initial minimum fluorescence to maximum fluorescence (F_0/F_m) ratio, indicating superior energy conservation capacity. Under increasing salinity, 1103 Paulsen maintained stable energy dissipation mechanisms, showing minimal increases in heat and fluorescence per reaction center (Dio/RC) values, even at 75 mM NaCl. M2 displayed pronounced changes in dissipation parameters, with substantial increases in non-photochemical quenching (Vj). R110 and M4 showed intermediate responses, with M4 exhibiting progressive increases in energy dissipation in the form of heat and fluorescence per cross-section (Dio/CSo) and R110 maintaining moderate dissipation levels until 50 mM NaCl.

Concerning the photosynthetic performance evaluation (Figure 3c), 1103 Paulsen demonstrated superior capacity under control conditions, with the highest performance index on an absorption basis (PI abs) and maximum quantum efficiency of PSII when all

reaction centers were open (F_v/F_m). Under salinity stress, it maintained stable photosynthetic efficiency even at 50 mM NaCl, showing minimal reductions in ETo/RC and φ(Po). M4 exhibited a severe decline in photosynthetic parameters, particularly in the F_v/F_0 ratio, while R110 maintained moderate efficiency until 50 mM NaCl. M2 showed progressive deterioration with increasing salinity, evidenced by declining PI abs and F_v/F_m values. These patterns align with genotype-specific salt tolerance levels, highlighting the robust photosynthetic machinery of 1103 Paulsen's under stress conditions.

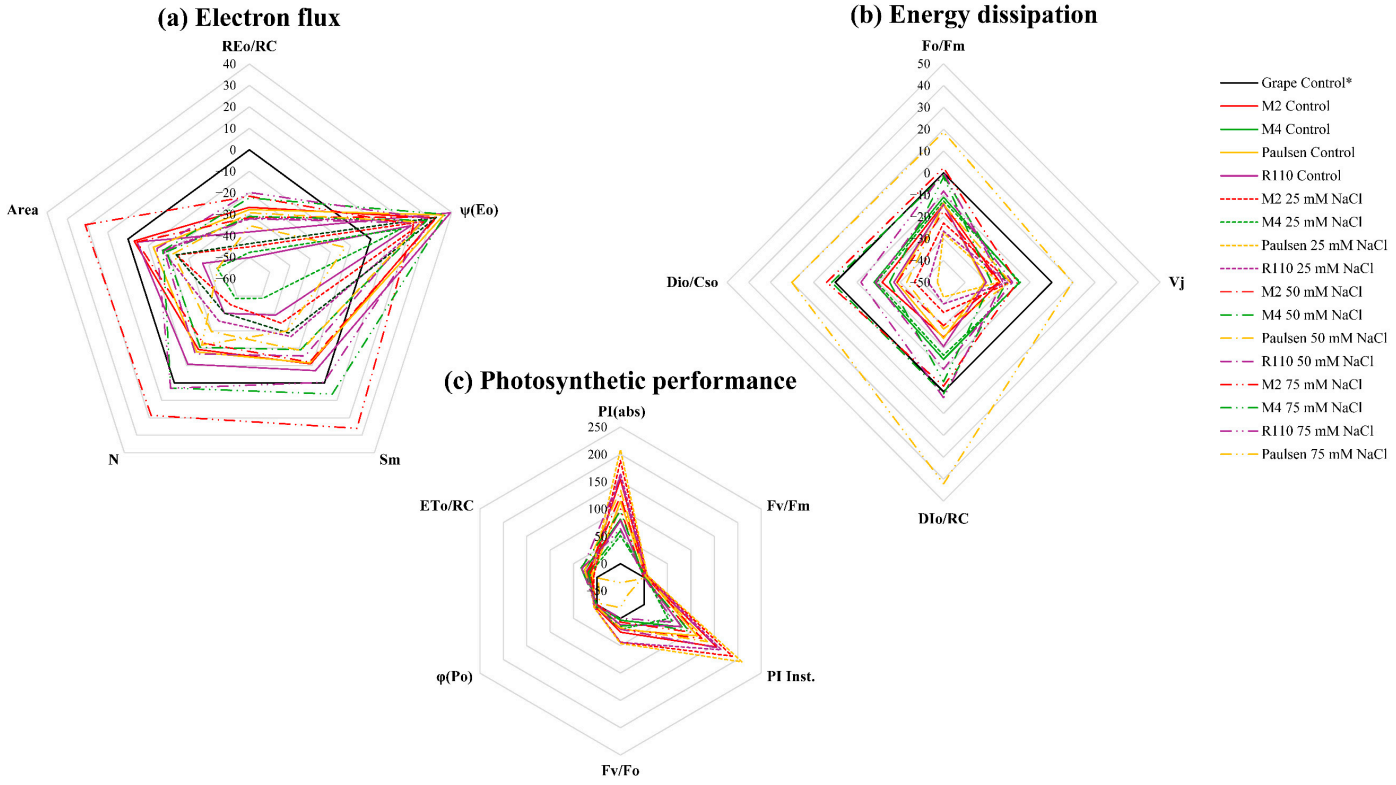

Figure 3. (**a**) Electron flux, (**b**) energy dissipation, and (**c**) photosynthetic performance for the different rootstocks as a function of salinity at the end of the experiment. "Grape control*" represents the average of all rootstock genotypes in April. Area represents the area above the fluorescence induction curve between the minimum fluorescence (F_0) and the maximum fluorescence (F_m) and is related to the pool size of electron acceptors in the photosynthetic electron transport chain. F_v/F_m is the maximum quantum efficiency of photosystem II (PSII) when all reaction centers are open. Vj represents the relative variable fluorescence at the J-step of the OJIP fluorescence transient and provides information about the reduction state of the primary quinone electron acceptor (QA). Sm is the normalized total complementary area above the OJIP transient and is related to the energy needed to close all PSII reaction centers. N represents the turnover number of QA, which is the number of times QA is reduced and oxidized during the measurement. DIo/RC is the energy dissipated in the form of heat and fluorescence per reaction center. ETo/RC represents the electron transport rate per reaction center. REo/RC is the rate of electron transport beyond QA per reaction center. φ(Po) is the maximum quantum yield of primary photochemistry. ψ(Eo) represents the efficiency with which a trapped exciton can move an electron into the electron transport chain beyond QA. DIo/CSo is the energy dissipated in the form of heat and fluorescence per cross-section. PI(abs) is the performance index on an absorption basis, which combines several fluorescence parameters to provide an overall measure of the performance of PSII.

Regarding the impact of increasing salinity levels on photosynthetic parameters across rootstock genotypes, the efficiency of photosystem II (Figure S7a) progressively decreased, as evidenced by reductions in F_v/F_m, PI abs, and ETR/RC values with increasing salinity, indicating reduced photochemical efficiency. Energy and electron transport parameters

(Figure S7b) showed a decline in electron flow (area, Sm, and N values) under higher salinity levels. Energy dissipation parameters (Figure S7c) revealed increased DIo/RC and Vj values with rising salinity, suggesting enhanced heat dissipation as a protective response to salinity stress. The 75 mM NaCl treatment caused the most pronounced alterations across all parameters compared to control conditions.

3.2.2. Gas Exchange

Statistical data on stomatal conductance across treatments and rootstock genotypes are presented in Table S8. Temporal analysis of stomatal conductance across salinity treatments revealed distinct patterns among grapevine rootstocks. Under control conditions, all rootstock genotypes displayed an initial increase in stomatal conductance, peaking between the second and third fortnight, with M2 and M4 showing the highest values, followed by 1103 Paulsen and R110 (Figure 4a). At 25 mM NaCl, R110 exhibited pronounced peaks in stomatal conductance that surpassed control values, while M4, M2, and 1103 Paulsen showed more moderate responses (Figure 4b). The 50 mM NaCl treatment generally induced lower stomatal conductance, with M4 showing high initial values followed by a sharp decline. In contrast, 1103 Paulsen maintained relatively stable stomatal conductance compared to the more variable responses observed in the other rootstock genotypes (Figure 4c). Under severe stress (75 mM NaCl), M4 and R110 initially displayed higher stomatal conductance followed by a rapid decline, while M2 and 1103 Paulsen maintained lower but more stable values (Figure 4d).

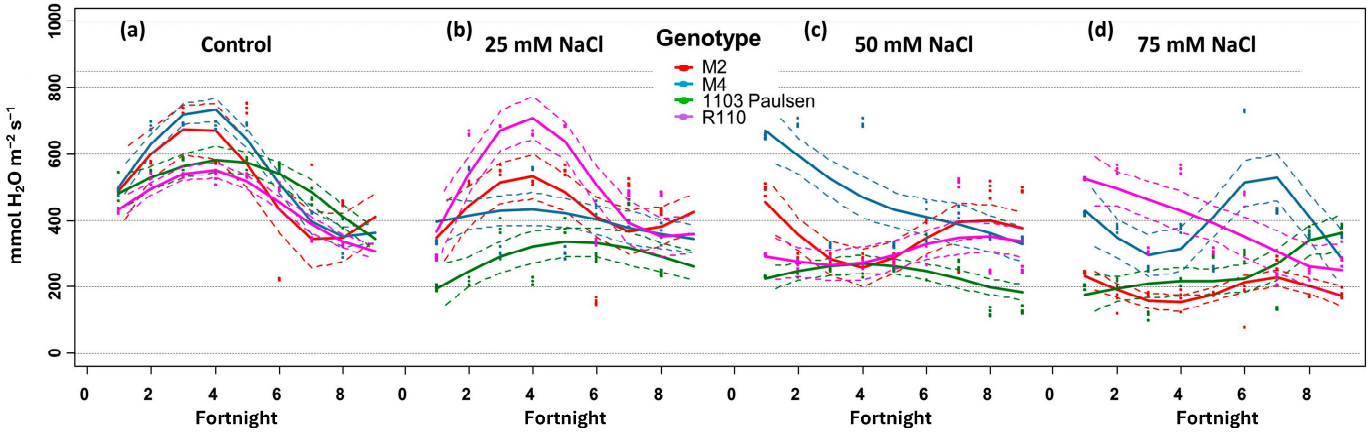

Figure 4. Spline representation of stomatal conductance (mmol H_2O m^{-2} s^{-1}) for each treatment as a function of rootstock genotype and date.

When temporal evolution is analyzed as a function of rootstock genotype rather than salinity dose, a clearer differentiation among genotypes emerges (Figure S8). Under control conditions, all genotypes exhibited similar patterns, with an initial increase. M2 exhibited high initial stomatal conductance under control and 25 mM NaCl treatments, peaking during the early weeks, but a progressive decrease was evident under high salinity levels, particularly at 75 mM NaCl (Figure S8a). M4 displayed more variable responses, notably featuring an unexpected spike in stomatal conductance at 75 mM NaCl around fortnight four, suggesting complex physiological adaptations (Figure S8b). In contrast, 1103 Paulsen demonstrated consistent responses across treatments, maintaining relatively stable stomatal conductance patterns even under increased salinity, indicating potentially higher salt tolerance (Figure S8c). R110 displayed erratic stomatal conductance patterns, with sporadic spikes at 50 mM NaCl and a pronounced tendency to decline at 75 mM NaCl (Figure S8d).

3.2.3. Soil–Plant Analysis Development (SPAD)

Statistical data on SPAD across treatments and rootstock genotypes are summarized in Table S9, revealing distinct rootstock genotype-specific patterns in chlorophyll content maintenance under varying salinity levels. Under control conditions (Figure 5a), M2 and R110 maintained relatively higher SPAD readings throughout most of the measurement period. All genotypes showed an initial increase in SPAD values during the first month. Between fortnights 2 and 6, there were gentle fluctuations, with a noticeable peak around fortnight 4. M4 and 1103 Paulsen generally displayed lower SPAD readings compared to M2 and R110. Around fortnight 6, a slight convergence of all genotypes occurred before they began to diverge again.

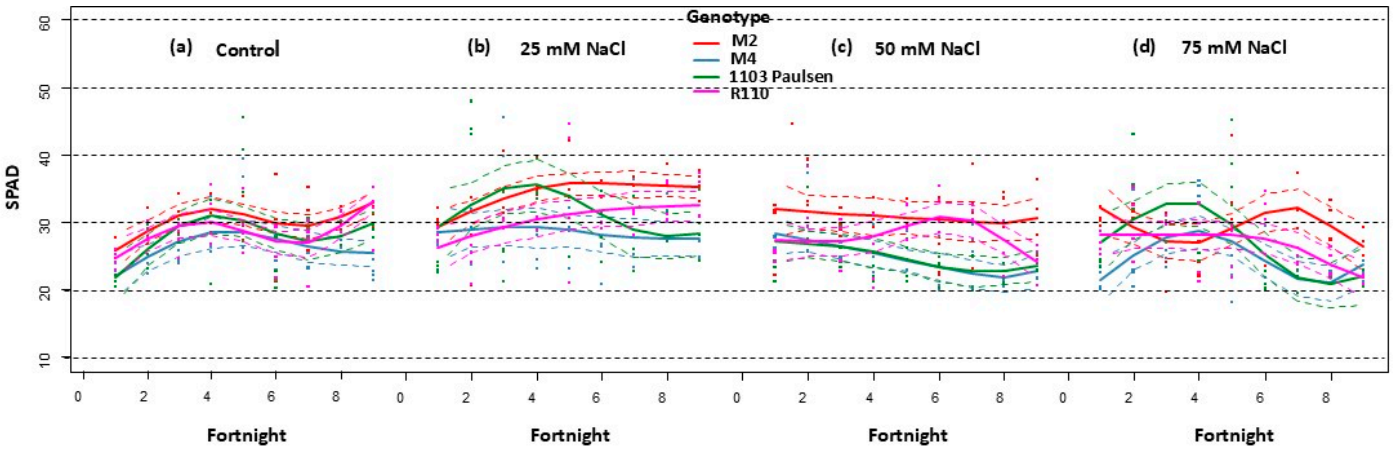

Figure 5. Spline representation of SPAD for each treatment as a function of genotype and date.

Under 25 mM NaCl (Figure 5b), M2 consistently exhibited the highest SPAD values. R110 followed closely, with its SPAD values improving towards the later fortnights. 1103 Paulsen demonstrated intermediate values, not consistently high, but stable across the experiment timeline. M4 maintained the lowest SPAD values throughout the experiment, indicating greater susceptibility to salinity.

Under 50 mM NaCl (Figure 5c), M2 and R110 exhibited the highest and most stable SPAD values throughout the experiment. 1103 Paulsen and M4 showed a constant decline, indicating varying salt tolerance levels.

Under 75 mM NaCl (Figure 5d), SPAD values showed a general decline across all genotypes, with clear differences in sensitivity. M2 maintained the highest SPAD values throughout the experiment. R110 showed intermediate values, slightly decreasing after fortnight 6 but still performing relatively well. 1103 Paulsen initially exhibited moderate SPAD values but sharply declined, indicating increased sensitivity to severe salinity. M4 consistently demonstrated the lowest SPAD values, highlighting its poor performance under these conditions.

When SPAD values are replotted as a function of rootstock genotype (Figure S9), it becomes apparent that higher salt concentrations (50 mM and 75 mM NaCl) resulted in lower SPAD values across all genotypes, though the magnitude of decline varied significantly. M2 maintained relatively stable SPAD values across treatments, with slightly higher values in control and 25 mM NaCl treatments (Figure S9a). M4 exhibited more variable responses, showing similar initial values across treatments but developing treatment-specific differences over time, with control and lower salt concentrations maintaining higher values (Figure S9b). 1103 Paulsen demonstrated the most dynamic response, featuring a notable increase in SPAD values around the fourth fortnight, particularly under 25 and 75 mM NaCl treatments, suggesting effective mechanisms for chlorophyll maintenance under

stress (Figure S9c). R110 showed consistent SPAD values across treatments with minimal fluctuations, indicating stable chlorophyll content maintenance regardless of salinity stress (Figure S9d).

3.3. Visual Symptoms

Under control conditions, all genotypes displayed vigorous growth with abundant green foliage and well-developed root systems (Figure 6).

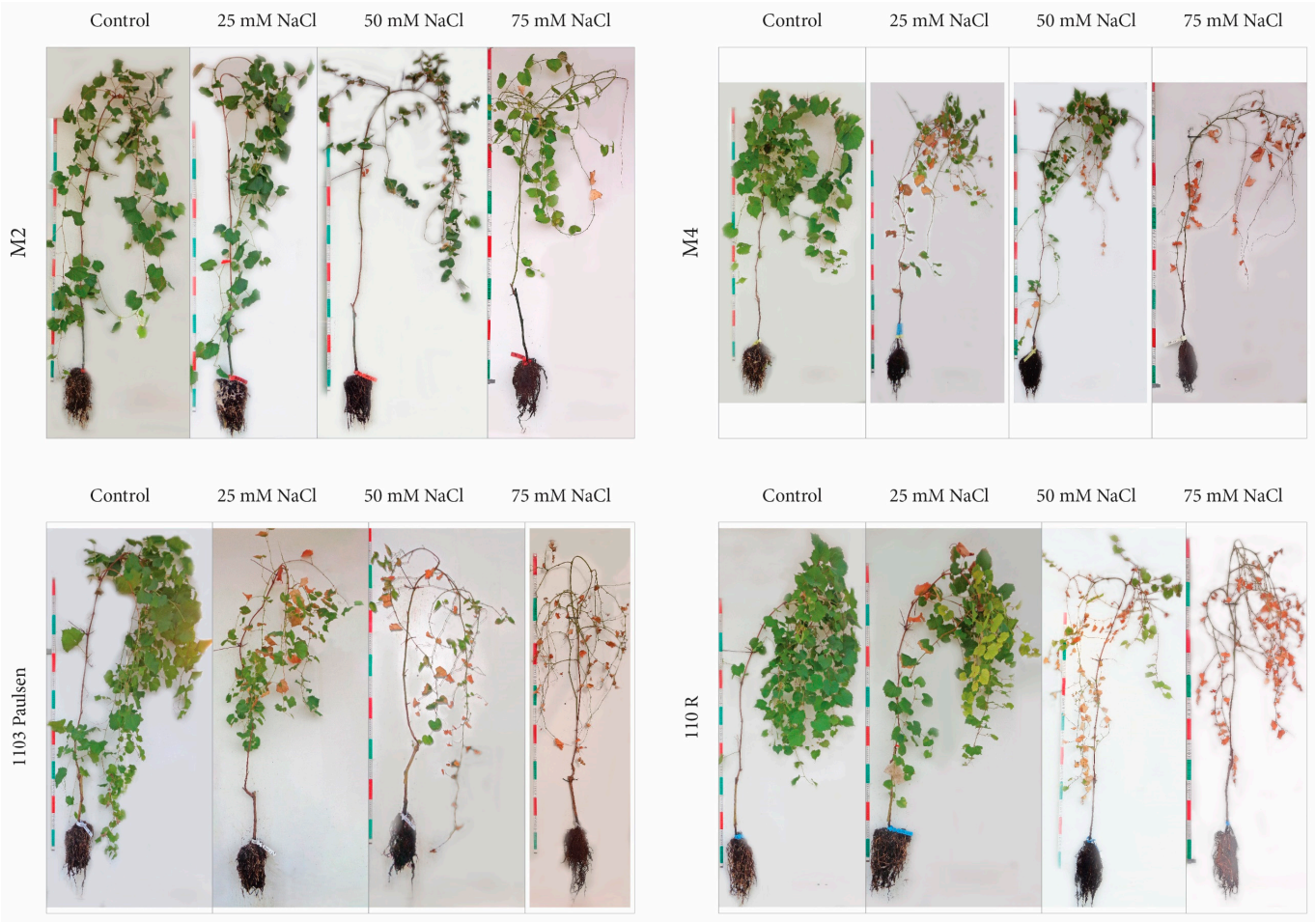

Figure 6. Visual aspect of the four rootstock genotypes subjected to the various salinity treatments at the end of the experiment. Only one replicate per treatment is shown.

At 25 mM NaCl, M2 maintained relatively robust growth, with minimal reductions in shoot length and leaf area, while 1103 Paulsen and R110 showed noticeable decreases in vegetative growth and some chlorosis. M4 exhibited a moderate reduction in plant size with early signs of salinity stress.

Under 50 mM NaCl, genotype differences became more pronounced. M2 sustained moderate growth with predominantly healthy green foliage despite a reduction in plant size. In contrast, 1103 Paulsen exhibited significant stunting and leaf discoloration, while R110 showed marked decreases in leaf number and increased stress symptoms. M4 displayed progressive deterioration, with evident chlorosis and reduced biomass.

At the highest salinity dose (75 mM NaCl), severe stress symptoms were observed across all genotypes, though with varying intensity. M2 maintained the best overall condition, with reduced but still considerable green foliage. 1103 Paulsen and R110 showed extreme stunting and defoliation, while M4 exhibited severe growth reduction and leaf discoloration.

Root system development generally decreased with increasing salinity across genotypes, though M2 maintained relatively better root development throughout treatments.

As the experiment progressed, salt toxicity symptoms became evident by the ninth fortnight and persisted until the experiment's conclusion. The most prominent symptom was observed in leaves, presenting as necrotic spots around the leaf edges (Figure 7a), which eventually progressed to whole-leaf death and defoliation.

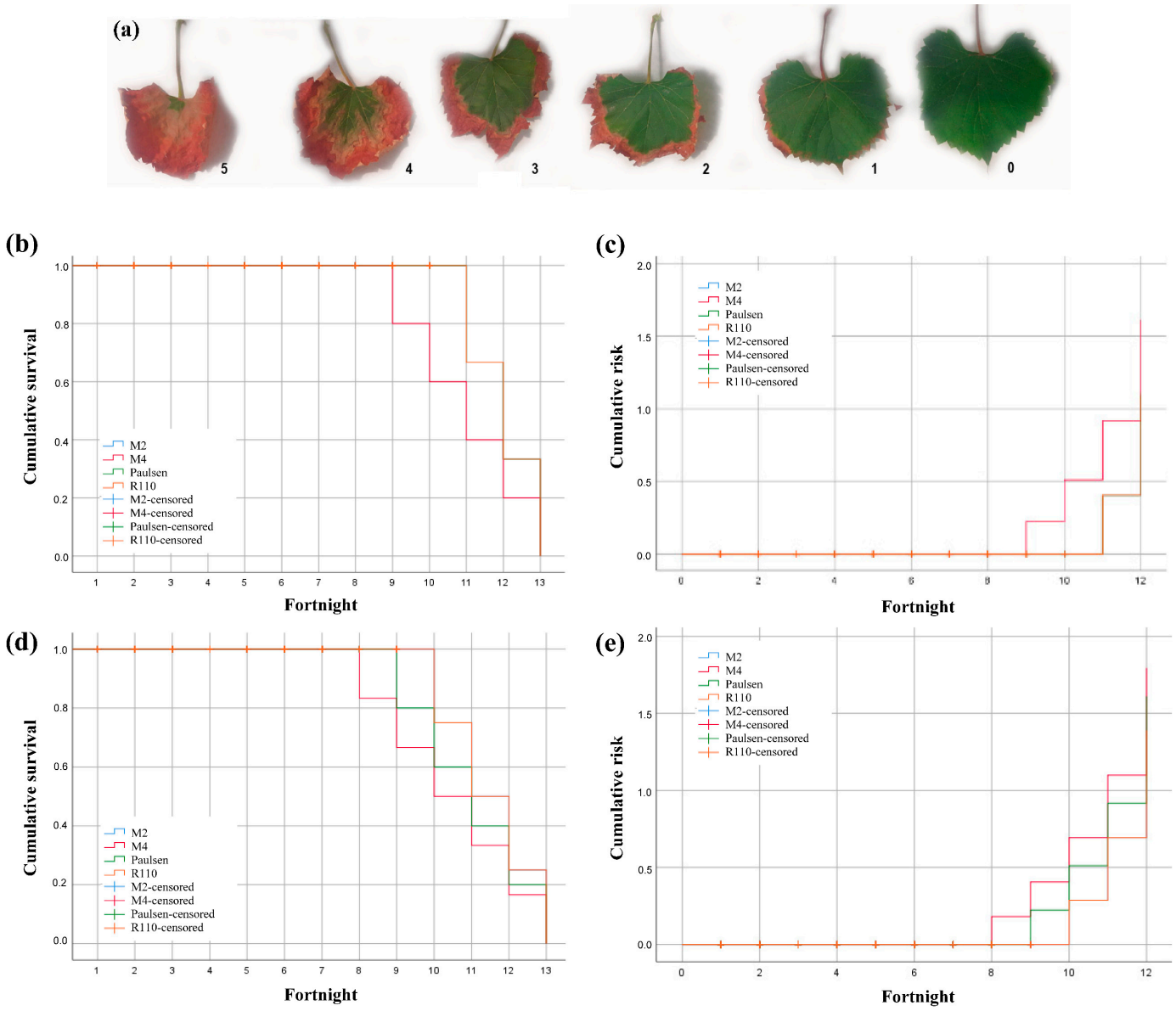

Figure 7. (**a**) Leaf damage level scale. Cumulative survival and cumulative risk of the different genotypes under (**b**,**c**) 50 mM and (**d**,**e**) NaCl 75 mM NaCl. Censoring is used in the legend in the sense that some information about individual survival time is available, but not the exact survival time.

Quantitative assessment of leaf damage (Table S10) revealed genotype-specific differences in stress symptom progression. No significant differences among genotypes were observed at control or 25 mM NaCl treatments. Under 50 mM NaCl, significant differences among genotypes emerged as early as fortnight 2 (p = 0.001), with M4 and R110 showing lower initial damage scores (mode value = 1) compared to 1103 Paulsen (mode value = 2) in fortnight 3. These significant differences later reemerged by fortnight 9 (p = 0.036), with R110 maintaining lower damage scores (mode value = 3) compared to other genotypes (mode values = 4–5). At 75 mM NaCl, genotypic differences became apparent from fortnight

1 (p = 0.001), with 1103 Paulsen showing higher damage scores during the early response phase. Plants under 75 mM NaCl reached maximum damage levels (5) by fortnight 8, with high mortality rates occurring from that point onwards, as evidenced in the survival analysis, discussed below.

Genotype responses to the 50 mM NaCl treatment varied (Figure 7b): M4 exhibited the highest sensitivity, with 20 stress-related events, while the other genotypes showed similar sensitivity, with 12 events each. Figure 7c demonstrates that M4 reached 50% of its stress events by the 10th fortnight, whereas the other genotypes reached this midpoint during the 12th fortnight, highlighting M4's heightened salinity stress susceptibility.

Under the 75 mM NaCl treatment, M4 showed the highest vulnerability, accumulating the most mortality events (24), followed by 1103 Paulsen with 20 events, and M2 and R110, which recorded 16 events each (Figure 7d,e). As for the onset of mortality, it occurred earliest in M4 and 1103 Paulsen, starting from the 8th and 9th fortnights, respectively, and continuing until the 12th fortnight.

3.4. Salinity-Induced Changes in Mineral Content and Ion Homeostasis

Our statistical analysis used the following three-way factorial model:

$$\text{Dependent variable (log-transformed)} = \text{Genotype} \times \text{Treatment} \times \text{Organ}$$

where the dependent variables were transformed using natural logarithm to meet normality assumptions, genotype represents the four rootstock types (1103 Paulsen, 110 Ritchter, M2, M4), treatment indicates the four salinity levels (0, 25, 50, and 75 mM NaCl), and organ refers to the different plant parts analyzed (roots, stems, leaves).

Logarithmic transformations were applied to correct for non-normal distribution in the data, enabling robust factorial ANOVA analyses. The diagnostic tests confirmed the validity of this statistical approach (Table S11). The analysis revealed significant effects for all three main factors (genotype, treatment, and organ) and their interactions (Table S12). To identify group differences, robust comparison methods were used, which are capable of addressing substantial heteroscedasticity and non-normality issues. Consequently, the original, untransformed variables were used for these comparisons, as this approach was deemed more appropriate given the data characteristics.

3.4.1. Calcium

Genotype-specific responses to salinity stress in terms of Ca^{2+} content were evident (Figure S10 and Table S13). Under control conditions, Ca^{2+} content was relatively uniform across genotypes, ranging from 2.91% in M2 to 3.03% in R110. At 25 mM NaCl, M4 showed slightly higher Ca^{2+} levels (3.12%), while 1103 Paulsen exhibited the lowest content (2.38%). The 50 mM NaCl treatment resulted in the highest Ca^{2+} accumulation across rootstock genotypes, particularly in M4 (3.36%) and M2 (3.01%). Under 75 mM NaCl, Ca^{2+} content generally decreased, with M2 showing the lowest values (2.25%) and M4 maintaining relatively higher levels (2.78%).

Calcium distribution also varied across plant organs (Figure S11 and Table S14). Root tissue consistently maintained the highest Ca^{2+} concentrations across all treatments, ranging from 4.82% to 6.44%, with the highest accumulation observed under the 50 mM NaCl treatment. Leaves demonstrated a clear response to increasing salinity, with the Ca^{2+} content progressively decreasing from 3.85% in the control to 1.92% under 75 mM NaCl treatment. Stem and wood tissues maintained relatively lower and more stable Ca^{2+} concentrations across treatments: stem Ca^{2+} content remained consistently low (1.29–1.55%), while wood tissue only showed slight increases with increasing salinity (from 1.58% to 1.87%).

3.4.2. Potassium

Genotype-specific responses to salinity stress were also observed in terms of K^+ content (Figure S12 and Table S15). Under control conditions, all rootstock genotypes exhibited similar K^+ levels, with values ranging from 3.67% in 1103 Paulsen to 3.95% in R110 (M2 and M4 had intermediate contents of 3.71% and 3.84%, respectively).

Exposure to 25 mM NaCl resulted in more pronounced variations in K^+ content among genotypes: 1103 Paulsen showed the lowest values (2.42%), while M2 maintained higher levels (3.18%). R110 and M4 displayed intermediate values of 3.08% and 2.55%, respectively.

As salinity was increased, in the 50 mM NaCl treatment, K^+ content further decreased across all genotypes, with values ranging from 1.92% (1103 Paulsen) to 2.59% (R110). M2 and M4 showed very similar contents under this treatment (2.25% and 2.26%, respectively).

Under the highest salinity level (75 mM NaCl), the pattern of K^+ distribution among genotypes remained consistent with that observed at 50 mM NaCl, though with generally lower values: R110 maintained the highest K^+ content (2.53%), followed by M4 (2.07%), M2 (1.98%), and 1103 Paulsen (1.94%).

The magnitude of K^+ content reduction from the control to the highest salinity treatment followed this sequence: 1103 Paulsen (47.3%) > M2 (46.4%) > M4 (46.1%) > R110 (35.9%). This relative ranking of rootstock genotypes in terms of K^+ content remained fairly consistent across treatments, with R110 generally maintaining higher levels and 1103 Paulsen showing lower values under increased salinity.

Regarding K^+ distribution across plant organs (Figure S13 and Table S16), leaves exhibited increased K^+ content with rising salinity, from 4.40% in the control to 5.47% under the 75 mM NaCl treatment. Conversely, stem tissue showed the highest initial K^+ content under control conditions (7.85%), but demonstrated a sharp decrease with increasing salinity, dropping to 3.93% at 25 mM NaCl and further decreasing to 2% under the 75 mM NaCl treatment. Root tissue also displayed a consistent decrease in K^+ content with increasing salinity, starting from 1.95% in control conditions and progressively declining to 0.50% under the 75 mM NaCl treatment. Wood tissue showed the lowest overall K^+ content, decreasing from 0.95% in the control to 0.54% under the most severe stress.

3.4.3. Chloride

Chloride content also evidenced genotype-specific responses to salinity stress (Figure S14 and Table S17). Under control conditions, all genotypes maintained relatively low Cl^- concentrations, ranging from 0.15% to 0.24%, with 1103 Paulsen showing marginally higher values. As salinity stress increased to 25 mM NaCl, Cl^- contents notably rose, with M4 and R110 showing similar elevated concentrations (approximately 0.89%), while M2 maintained the lowest levels (0.64%). Irrigation with a dose of 50 mM NaCl induced further increases, with 1103 Paulsen accumulating the highest Cl^- concentration (1.16%), followed closely by M4 (1.09%), while M2 and R110 showed moderate levels of around 0.90%. Under 75 mM NaCl, all genotypes exhibited their peak Cl^- concentrations, with M4 and 1103 Paulsen demonstrating the highest accumulation (1.87% and 1.81%, respectively), followed by R110 (1.54%), while M2 maintained the lowest levels (1.30%).

Chloride distribution also varied across plant organs (Figure S15 and Table S18). Leaves showed the most dramatic response to salinity, with the highest overall Cl^- accumulation, increasing from 0.08% under control conditions to 3.25% under 75 mM NaCl, representing a 40-fold increase. Stems exhibited the second-highest Cl^- accumulation, with concentrations rising from 0.26% at control to 1.94% at 75 mM NaCl (7.5-fold increase). Roots showed a more moderate response, with Cl^- levels increasing from 0.32% at control to 0.89% at 75 mM NaCl (three-fold increase). Wood tissue, with the lowest overall Cl^-

accumulation under control conditions (0.09%) demonstrated an intermediate response between those of stems and roots, with a five-fold increase (reaching 0.44% at 75 mM NaCl).

3.4.4. Sodium

Concerning the Na^+ content, genotype-specific responses to salinity stress were also detected (Figure S16 and Table S19). Under control conditions, all rootstock genotypes maintained low Na^+ concentrations, ranging from 0.20% (R110) to 0.26% (1103 Paulsen). Irrigation with the 25 mM NaCl treatment resulted in varied responses, with M4 and 1103 Paulsen showing higher accumulation (approximately 1.06% and 1.04%, respectively), representing a four-fold increase from control, while M2 and R110 demonstrated more moderate increases (0.73% and 0.81%, respectively), corresponding to about a three-fold rise from the control baseline. Under 50 mM NaCl, Na^+ levels further increased, with notably different patterns among genotypes: 1103 Paulsen accumulated the highest concentration (1.46%, a 5.5-fold increase compared to the control), followed by M4 (1.31%, 5.4-fold increase). M2 and R110 showed relatively lower, but still substantial, increases (1.21% and 1.18%, respectively, representing approximately a five-fold increase compared to the control). At 75 mM NaCl, M2 and M4 exhibited the highest Na^+ accumulation (approximately 1.65% in both genotypes, representing a seven-fold increase compared to the control), followed closely by R110 (1.58%, eight-fold increase), while 1103 Paulsen showed comparatively lower accumulation (1.48%, 5.6-fold increase).

With regard to Na^+ distribution across plant organs (Figure S17 and Table S20), it is worth noting that, under control conditions, roots showed the highest Na^+ content (0.37%), followed by stems (0.24%), leaves (0.20%), and wood tissue (0.13%). As salinity increased to 25 mM NaCl, stems demonstrated a dramatic increase to 1.73% (7.2-fold increase vs. the control), while leaves and roots showed moderate increases to 0.83% and 0.73%, respectively (approximately 4-fold increase), and wood maintained the lowest accumulation (0.36%, 2.8-fold increase). Under 50 mM NaCl treatment, stems continued to accumulate the highest Na^+ concentrations (2.12%, 8.9-fold increase vs. the control), followed by roots (1.32%, 3.5-fold increase), leaves (1.13%, 5.8-fold increase), and wood (0.59%, 4.5-fold increase). At 75 mM NaCl, stems maintained the highest Na^+ content (2.37%, 9.9-fold increase vs. the control), while roots and leaves showed similar levels (1.60% and 1.54%, respectively, representing 4.3-fold and 7.8-fold increases), and wood exhibited the lowest accumulation (0.84%, 6.5-fold increase).

3.4.5. Potassium/Sodium Ratio

In connection with the K^+/Na^+ ratio, genotype-specific responses to salinity stress are summarized in Figure S18 and Table S21. Under control conditions, R110 maintained the highest K^+/Na^+ ratio (35), substantially higher than those of the other rootstock genotypes, whose ratios ranged from 15.77 to 16.94. As salinity increased to 25 mM NaCl, all genotypes showed a dramatic decrease in K^+/Na^+ ratios, though M2 and R110 maintained relatively higher ratios (4.36 and 4.48, respectively) compared to M4 and 1103 Paulsen (approximately 2.7 for both). The decline continued under the 50 mM NaCl treatment, with most genotypes showing ratios between 1.5 and 1.8, except for R110, which maintained a slightly higher ratio (2.71). Under 75 mM NaCl, all genotypes exhibited their lowest K^+/Na^+ ratios (1.18–1.65), with minimal differences between genotypes. The reduction in K^+/Na^+ ratios from the control conditions to the 75 mM NaCl irrigation dose was most dramatic in R110 (94% decrease), followed by M4 and M2 (91% and 93% decrease, respectively), while 1103 Paulsen showed a slightly lower overall reduction (92%).

In line with the observations made for the cations, K^+/Na^+ ratio distribution also varied across plant organs (Figure S19 and Table S22). Under control conditions, stems

exhibited the highest K^+/Na^+ ratio (39.93), followed by leaves (25.19), while wood and roots maintained lower ratios (7.73 and 5.27, respectively). At 25 mM NaCl, substantial decreases were found across all organs, though leaves maintained the highest ratio (7.28, 71% decrease vs. the control), followed by stems (2.97, 93% decrease), wood (2.21, 71% decrease), and roots (1.76, 67% decrease). Under the 50 mM NaCl treatment, leaves continued to maintain the highest K^+/Na^+ ratio (5.03), while other organs showed marked decreases, with stems at 1.15, wood at 0.94, and roots at 0.72. At 75 mM NaCl, all organs exhibited their lowest K^+/Na^+ ratios, with leaves maintaining relatively higher values (3.64) compared to stems (0.88), wood (0.66), and roots (0.32). Stem tissue exhibited the greatest decrease in K^+/Na^+ ratios, declining by 98% when comparing control conditions to the 75 mM NaCl treatment, while leaves showed a more moderate reduction (86%), and roots and wood displayed intermediate responses (94% and 91% decrease, respectively).

3.4.6. Calcium/Sodium Ratio

Genotype-specific responses to salinity stress were evident (Figure S20 and Table S23). Under control conditions, R110 maintained the highest Ca^{2+}/Na^+ ratio (17.91), while other genotypes showed similar ratios ranging from 12.27 to 12.94, indicating R110's superior ability to maintain calcium uptake over sodium under non-stressed conditions.

At 25 mM NaCl, all genotypes showed substantial decreases in Ca^{2+}/Na^+ ratios, though M4 maintained a relatively higher ratio (5.07, 61% decrease from control), followed by M2 (4.37, 66% decrease) and R110 (4.19, 77% decrease), with 1103 Paulsen showing the lowest ratio (3.58, 71% decrease). Significant differences were found at this dose ($p > 0.05$). Under 50 mM NaCl, further decreases were observed, with M4 maintaining the highest ratio (3.33), followed by R110 (2.96) and M2 (2.60), with 1103 Paulsen showing the lowest values (2.10). At 75 mM NaCl, all genotypes exhibited their lowest Ca^{2+}/Na^+ ratios, with M4 maintaining relatively higher values (2.23, 83% decrease from control), followed by 1103 Paulsen (1.94, 84% decrease) and R110 (1.83, 90% decrease), with M2 showing the lowest ratio (1.57, 88% decrease). The overall reduction in Ca^{2+}/Na^+ ratios from control to 75 mM NaCl was most pronounced in R110 (90% decrease), while M4 showed the most moderate reduction (83% decrease), suggesting better calcium retention capacity under severe salinity stress.

The calcium/sodium ratio distribution also varied across plant organs (Figure S21 and Table S24). Under control conditions, leaves exhibited the highest Ca^{2+}/Na^+ ratio (22.23), followed by roots (14.08) and wood (12.74), while stems showed substantially lower ratios (6.85). This indicates strong differential ion accumulation patterns among organs under non-stressed conditions. With the transition to the 25 mM NaCl treatment, all organs showed marked decreases, though roots maintained the highest ratio (7.33, 48% decrease from control), followed by wood and leaves with similar ratios (4.48 and 4.34, respectively, representing 65% and 80% decreases), while stems showed the most dramatic reduction (1.06, 85% decrease). Under 50 mM NaCl, roots continued to maintain the highest Ca^{2+}/Na^+ ratio (5.24), followed by wood (3.08), leaves (1.90), and stems (0.76). At 75 mM NaCl, all organs exhibited their lowest Ca^{2+}/Na^+ ratios, with roots maintaining relatively higher values (3.42, 76% decrease from control), followed by wood (2.29, 82% decrease) and leaves (1.28, 94% decrease), with stems showing the lowest ratio (0.57, 92% decrease). The overall reduction in Ca^{2+}/Na^+ ratios from control to 75 mM NaCl was most dramatic in leaves and stems (94% and 92% decreases, respectively), while roots and wood showed more moderate reductions (76% and 82%, respectively).

3.5. Principal Component Analysis

Two factors from the PCA explained 66.53% of the total variance in grapevine rootstock responses to salinity stress. The represented variables included growth parameters (shoot length and trunk diameter), gas exchange (stomatal conductance), chlorophyll content (SPAD), and salinity-induced damage. It should be clarified that the ordinal variable salinity-induced damage was included due to its biological relevance in the study, as it represents an estimate of the damage severity, which can be associated with continuous physiological measures (SPAD, stomatal conductance). To ensure the compatibility of the scales, a correlation matrix based on Spearman's coefficient was employed. This method is suitable for integrating continuous and ordinal variables by means of ranks. This approach allowed us to identify common patterns and explore interactions between variables in a multivariate space.

The first component (D1), which explained 38.96% of the total variance, was strongly associated with variables related to physical growth, such as shoot length and trunk diameter, indicating that it represents a "physical growth factor". The second component (D2), which explained 27.57% of the variance, was mainly related to salinity-induced damage and stomatal conductance, which represents physiological measures of transpiration. This suggests that D2 reflects a "physiology and damage factor".

The biplot (Figure 8) revealed clear relationships between the measured parameters, with shoot length and trunk diameter showing strong correlations along the D1 axis, suggesting their coordinated response to salinity stress conditions. SPAD values, representing chlorophyll content, demonstrated a moderate positive correlation with D1, suggesting that leaf chlorophyll content changes were somewhat aligned with growth responses under salinity stress. As for the porometer readings (stomatal conductance), they showed a strong positive correlation along D2, while damage showed a strong negative correlation. This suggests an inverse relationship between these parameters under salinity stress conditions. The salinity-induced damage observed in the plants directly affected stomatal functionality, reducing transpiration and gas exchange as measured by the porometer. The orthogonal relationship between porometer readings and growth parameters indicates that stomatal conductance responses to salinity are regulated independently from plant growth responses.

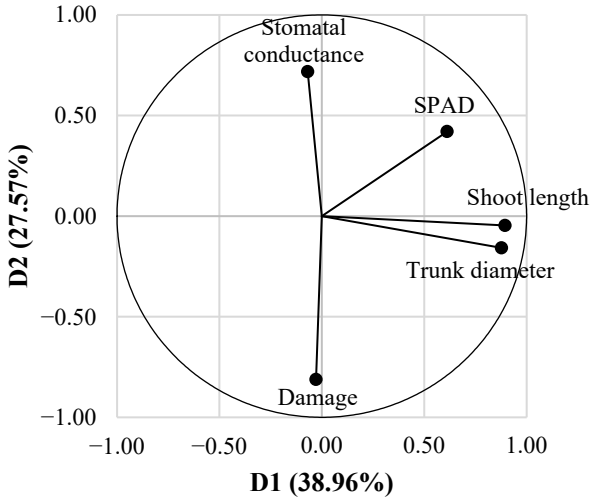

Figure 8. Biplot of the principal component analysis (PCA) based on Spearman's correlation matrix. The axes represent the first two principal components (D1 and D2) along with the percentage of the total variance explained. The direction and length of the arrows indicate the contribution of each variable to the components.

The varying lengths of the vectors demonstrated the differential sensitivity of these parameters to salinity stress in grapevines. Growth parameters contributed more strongly to the explained variance, as indicated by their longer vectors, while parameters such as the stomatal conductance contributed to a lesser extent.

4. Discussion

4.1. Growth Responses Under Salinity Stress

4.1.1. Fresh and Dry Weight

Salinity stress reduces fresh and dry weights by disrupting water uptake and ion homeostasis [54], with fresh weight indicating short-term osmotic effects and dry weight reflecting lasting biomass impacts. M2 and R110 maintained moderate fresh and dry biomass across salinity levels, suggesting salt tolerance through ion exclusion and compartmentalization [55], in contrast to M4 and 1103 Paulsen, especially under 50−75 mM NaCl. R110's biomass stability is attributed to efficient Na^+ exclusion and sequestration, mitigating cytotoxic effects in photosynthetic tissues, supporting osmotic balance, and preventing ion toxicity in leaves and stems [56]. 1103 Paulsen's superior biomass retention compared to M4 would be linked to effective ion exclusion and selective ion transport [57].

Leaf biomass reduction under high salinity aligns with previous findings [24], while superior stem biomass retention in M2 and R110 is attributed to structural and physiological adaptations for water retention under osmotic stress. Roots and stems enhance salinity resilience by compartmentalizing ions, mitigating toxic concentrations in sensitive tissues [57].

4.1.2. Shoot Length

The observed reduction in shoot growth across all studied genotypes under increasing salinity is likely a result of osmotic stress adaptation [58]. M2 experienced a significant reduction in shoot length under high salinity, likely due to impaired photosynthetic efficiency [17]. 1103 Paulsen's stable shoot length across varying salinity levels aligns with previous research on salt-tolerant rootstocks, such as Ramsey and 1103 Paulsen, possessing efficient ion exclusion mechanisms [59]. The relatively stable shoot length observed in R110 and 1103 Paulsen may also be due to their ability to maintain osmotic balance [60] and effective ion compartmentalization [61].

4.1.3. Trunk Diameter

Under salinity stress, trunk growth reduces due to osmotic and ionic stress [54]. Trunk growth stability is associated with efficient nutrient management, particularly of K^+ and Ca^{2+} [1]. M2 and R110 exhibited better trunk growth under salinity compared to M4 and 1103 Paulsen, suggesting enhanced structural tolerance achieved through ion exclusion, osmotic adjustment mechanisms, and superior nutrient management. The poor growth observed for M4 in this study contradicts previous reports by Porro et al. [25] and Meggio et al. [24], where it demonstrated resilience in high-stress environments. R110's ability to sustain trunk growth better than M2 under high salinity suggests effective osmotic adjustment mechanisms [56]. 1103 Paulsen's stable trunk diameter at 75 mM NaCl aligns with previous findings on salt-tolerant rootstocks maintaining structural growth under saline conditions [1,62].

4.2. Physiological Adaptations to Salinity Stress

4.2.1. Fluorimetry

Under salinity stress, M2 showed a marked decline in maximum quantum yield (φ(Po)) and electron transport probability (ψ(Eo)), indicating vulnerability in its photosynthetic

machinery [63]. 1103 Paulsen maintained stable electron transport characteristics, reflecting salt-tolerant plants' ability to maintain higher electron transport rates and photochemical efficiency [60].

The observed differences in electron transport chain efficiency among genotypes, particularly M2 and M4's sensitivity, are consistent with the salinity stress disruption of PSII functionality through impaired electron transport components [37]. The energy dissipation analysis revealed additional genotype-specific patterns under salinity stress. 1103 Paulsen exhibited the highest initial F_0/F_m ratio and sustained energy conservation even at 75 mM NaCl, consistent with salt-tolerant genotypes enhancing non-photochemical quenching to protect PSII from oxidative damage [64]. The minimal increases in Dio/RC values observed in 1103 Paulsen under high salinity further confirm its effective use of these protective mechanisms.

M2 showed significant increases in energy dissipation (Dio/RC) and elevated Vj values under high salinity, indicating less efficient photoprotective mechanisms [65]. R110 maintained stable electron transport efficiency until 50 mM NaCl, consistent with moderate salt tolerance linked to partial ion exclusion and reactive oxygen species (ROS) scavenging [55]. However, R110's electron transport gradually decreased under severe salinity, indicating some tolerance, though not as robust as that demonstrated by 1103 Paulsen.

4.2.2. Gas Exchange

The general reduction in conductance at 50 and 75 mM NaCl across all genotypes suggests osmotic and oxidative stress adaptations [66]. M2's sharp decline in conductance at 75 mM NaCl aligns with previous findings on elevated salinity disrupting water uptake [58]. Additionally, prolonged exposure leads to salt toxicity (hyper-ionic stress) and worsens water imbalances (hyper-osmotic stress), requiring complex survival adaptations. This adaptation likely reflects M2's response of conserving water under severe salinity by reducing transpiration.

1103 Paulsen's stable stomatal conductance across treatments suggests robust salt tolerance mechanisms, potentially through effective ion exclusion and osmotic adjustment [57]. R110's intermittent conductance spikes under high salinity could indicate suboptimal ion regulation [66]. M4's conductance spike at 75 mM NaCl suggests an adaptive response of temporarily optimizing CO_2 uptake [24].

4.2.3. Soil–Plant Analysis Development (SPAD)

M2 and 1103 Paulsen displayed higher stability across treatments, suggesting inherent resilience in maintaining chlorophyll under stress. The gradual SPAD decline in M4 and R110 at higher salinity levels suggests greater salt sensitivity, with increased chlorophyll degradation under stress [65].

1103 Paulsen's dynamic increase under 25 mM NaCl indicates an adaptive response to mild stress, likely through mechanisms that stabilize chlorophyll content [58]. Its sustained SPAD levels under both moderate and high salinity support its robust antioxidant mechanisms for minimizing oxidative damage [67]. M2's stable SPAD values of M2 across salinity levels suggest inherent chlorophyll stability mechanisms, potentially related to efficient ion exclusion or osmotic adjustment [66].

4.3. Visual Symptoms

All genotypes demonstrated robust growth and development under control conditions, with lush foliage and robust root systems, indicative of optimal conditions for photosynthetic and metabolic activities.

At 25 mM NaCl, M2 maintained relatively robust growth, with minimal reductions in shoot length and leaf area, while 1103 Paulsen, R110, and M4 showed noticeable growth

reductions and leaf chlorosis, indicating moderate sensitivity. This early chlorotic response can be attributed to the osmotic stress that salinity imposes on leaf tissues, leading to decreased chlorophyll synthesis [61].

Under 50 mM NaCl, 1103 Paulsen and R110 exhibited considerable stunting and leaf discoloration, signifying limited capacity to exclude salt ions, while M2 and M4 demonstrated moderate tolerance, with healthy foliage and reduced, but sustainable, plant size. This resilience is indicative of efficient ion regulation [13].

At 75 mM NaCl, 1103 Paulsen and R110 experienced extreme stunting, defoliation, and reduced root development, reflecting their physiological limits. M4 exhibited severe defoliation, tissue damage, and stem architecture with a smaller root system, pointing to salt-induced nutrient imbalance and dehydration in leaf tissues [1]. M2 maintained comparatively better condition, retaining some green foliage, indicative of its relative resilience.

Leaf necrosis and other toxicity symptoms were most pronounced in M4 and 1103 Paulsen towards the 10th fortnight, correlating with increased mortality [68]. This high susceptibility in M4 suggests poor ion exclusion and regulation under salinity. El-Salhy et al. [68] reported similar patterns in 1103 Paulsen, R110, and Salt Creek, in which poor ionic management led to extensive tissue damage under high salinity.

In terms of survival, M4 showed the highest mortality rate under 50 mM and 75 mM NaCl, consistent with previous findings on rootstocks (RS-19 and Salt Creek) exhibiting rapid mortality under extended salinity exposure due to their inability to maintain ion homeostasis [61].

4.4. Salinity-Induced Changes in Mineral Content and Ion Homeostasis

4.4.1. Calcium

Under control conditions, Ca^{2+} levels were relatively consistent for all rootstock genotypes. Upon salinity increase to 25 mM NaCl, Ca^{2+} content increased in the case of M4, while R110, M2, and 1103 Paulsen showed decreasing trends, suggestive of a reduced ion uptake strategy [54]. These changes may be linked to root architecture differences and calcium transporter expression [69]. At 50 mM NaCl, Ca^{2+} levels peaked across genotypes, with M4 and R110 retaining the highest levels, suggesting Ca^{2+} uptake to mitigate ionic imbalance [70]. At 75 mM NaCl, Ca^{2+} levels generally declined, with M2 showing the lowest value. M4's relative Ca^{2+} content stability across treatments is consistent with its classification as a moderately salt-tolerant genotype [24]. This stability suggests effective vacuolar sequestration mechanisms that maintain cellular Ca^{2+} homeostasis under stress [71].

Concerning plant organs' Ca^{2+} contents, roots consistently had the highest content, remaining stable across treatments, highlighting their central role in Ca^{2+} storage and ion regulation under stress [72]. In contrast, leaves displayed the greatest sensitivity, with Ca^{2+} levels decreasing as a result of Na^{+}-induced displacement [73]. Wood and stems showed much lower Ca^{2+} levels, indicating a structural rather than regulatory function [60].

4.4.2. Potassium

K^{+} content decreased with increasing salinity across all genotypes, consistent with high Na^{+} levels interfering with K^{+} uptake and transport [74]. Under 75 mM NaCl, R110 maintained the highest K^{+} content, followed by 1103 Paulsen, while M2 and M4 showed the lowest K^{+} retention, indicating differential activation of K^{+}-specific transport systems under severe stress conditions [75] and suggesting adaptive responses to maintain osmotic balance and support photosynthesis under stress conditions [76].

Organ-specific K^{+} distribution patterns showed that leaves maintained the highest K^{+} concentrations, potentially as part of an osmotic adjustment response [72]. Stems

and roots showed significant decreases in K^+ content, aligning with K^+ prioritization to photosynthetic tissues under stress [55]. Walker et al. [59] found a negative correlation between K^+ and Na^+ in the trunk wood of Chardonnay on C5 and 101-14 rootstocks, suggesting that higher K^+ levels might help mitigate Na^+ accumulation. These K^+ retention differences among genotypes and organs affect various physiological processes, including osmotic adjustment, enzyme activation, and stomatal regulation [65].

4.4.3. Chloride

Rootstock selection affects Cl^- exclusion and plant accumulation. At 75 mM NaCl, M2 and R110 accumulated less Cl^- than M4 and 1103 Paulsen, suggesting more effective Cl^- exclusion mechanisms [59] and reflecting genotypic variations in Cl^- exclusion [77], which become more pronounced under severe stress [17].

R110's more limited Cl^- accumulation indicates enhanced salinity resistance [54], while 1103 Paulsen's intermediate performance suggests varied tolerance mechanisms beyond Cl^- exclusion. Lo'ay and El-Ezz [62] observed lower Cl^- accumulation across organs in 1103 Paulsen compared to 140 Ru. Among M-series rootstocks, M4 exhibited higher Cl^- content than M2, despite previous reports on its moderate resistance [22,24].

Regarding organ distribution, leaf Cl^- peaked at 3.25% under 75 mM NaCl, impairing photosynthetic efficiency [12,55]. Wood showed a minimal increase, while root Cl^- moderately increased, indicating partial uptake barrier function. Ion transporters contribute to root exclusion but may become insufficient at higher salinity [78]. Tregeagle et al. [77] observed varying chloride transport mechanisms among rootstocks, with better excluders showing reduced root-to-shoot transfer.

4.4.4. Sodium

Genotypic variations among the studied rootstocks emerged under moderate salinity (25–50 mM NaCl), with M4 and 1103 Paulsen showing higher Na^+ accumulation than M2 and R110, reflecting varying root-level exclusion capacities [16,54]. The sharp rise at 50 mM NaCl indicates a threshold at which exclusion mechanisms become less effective [57]. At 75 mM NaCl, Na^+ content converged among genotypes, suggesting shared internal compartmentalization mechanisms [71,79].

R110 and M2's lower Na^+ accumulation under moderate stress, likely through enhanced expression of plasma membrane Na^+/H^+ antiporters in root tissues, aligns with previous findings on superior Na^+ exclusion capabilities [78].

Regarding organ distribution, stems served as primary Na^+ reservoirs, protecting photosynthetic tissues [12]. Lower leaf Na^+ levels indicate active transport regulation to preserve photosynthetic capacity [16,80]. Roots exhibited substantial accumulation (1.60% at high salinity), reflecting their buffering role [54], while wood showed minimal involvement in salinity regulation.

4.4.5. Potassium/Sodium Ratio

The K^+/Na^+ ratio serves as a critical indicator of ion homeostasis in plants under salinity stress, reflecting their capacity to maintain cytosolic K^+ while excluding or compartmentalizing Na^+ [71]. Under control conditions, R110 and 1103 Paulsen displayed the highest K^+/Na^+ ratios, demonstrating effective Na^+ exclusion [80]. At 25 mM NaCl, M2 and R110 maintained higher ratios compared to M4 and 1103 Paulsen, indicating superior Na^+ exclusion through selective ion channels [78]. At 50 mM NaCl, ratios declined more pronouncedly in M4 and 1103 Paulsen. Under 75 mM NaCl, differences decreased, with R110 and M2 showing marginally higher ratios, suggesting saturation of selective ion transport mechanisms at high salinity [13].

With regard to differences among plant organs, leaves exhibited the highest initial K^+/Na^+, crucial for photosynthetic processes, declining to approximately 2.1 at 75 mM NaCl, reflecting both Na^+ leakage and K^+ efflux under stress [78]. Roots displayed lower ratios, reflecting direct exposure to saline conditions while maintaining active K^+ uptake and Na^+ exclusion mechanisms [81]. Stems and wood showed intermediate ratios, supporting Na^+ sequestration to protect photosynthetic tissues [60].

4.4.6. Calcium/Sodium Ratio

Under control conditions, all genotypes exhibited high Ca^{2+}/Na^+ ratios, with R110 showing the highest Ca^{2+} homeostasis [81]. Ratios declined in all genotypes under 25 mM NaCl, though M2 and R110 maintained relatively higher values, tentatively associated with increased expression of Ca^{2+}-ATPases and/or CAX transporters [55]. At 50 mM NaCl, decreased ratios indicated reduced Ca^{2+} availability and increased ion competition [56], with more pronounced declines in M4 and 1103 Paulsen. Under 75 mM NaCl, differences between genotypes diminished. The R110 and M2 genotypes maintained relatively higher Ca^{2+} levels, correlating with superior vacuolar Na^+ compartmentalization [76].

Organ-specific analysis showed that leaves had the highest initial Ca^{2+}/Na^+ ratios, crucial for stomatal regulation [66], but these ratios significantly decreased at 75 mM NaCl. Roots initially showed high ratios, providing oxidative stress protection [72]; stems exhibited the lowest ratios, functioning as Na^+ reservoirs [71]; and wood showed moderate initial ratios with limited regulation capacity [58].

4.5. Principal Component Analysis

Principal Component Analysis of rootstock responses revealed complex interactions among various physiological parameters, reflecting the multifaceted nature of salt tolerance mechanisms [54,56].

The first component, representing overall plant size and health, included shoot length, trunk diameter, and SPAD values, corroborating observations on how salinity affects both growth and photosynthetic capacity [68]. The second component revealed an important contrast between plant damage and stomatal conductance, consistent with findings regarding differential response kinetics to salinity stress [58]. This inverse relationship suggests a potential trade-off between maintaining gas exchange and minimizing tissue damage under saline conditions. The positioning of the damage variable, showing negative correlations with most other parameters, aligns with previous findings correlating visible damage symptoms with reduced growth and physiological function [55,82].

The variability explained by the model reflects genotypic differences in salt tolerance, consistent with demonstrated variation in physiological responses among grapevine genotypes [12,59].

4.6. Genotype Performance Comparison

The four grapevine rootstocks exhibited distinct responses to salinity stress, revealing diverse adaptation mechanisms. M2 demonstrated superior performance in growth parameters, maintaining the longest shoots and largest trunk diameter under stress conditions, while showing remarkable stability in chlorophyll content across treatments. However, its photosynthetic efficiency significantly declined under high salinity, suggesting a potential trade-off between growth maintenance and photosynthetic performance. This apparent paradox reflects strategic resource allocation: M2 maintains growth through enhanced mobilization of stored carbohydrates from woody tissues (evidenced by a 36.1% reduction in wood dry weight under stress) and increased sink strength in growing tissues (supported by superior fresh weight retention). The declining photosynthetic efficiency, marked by increased non-photochemical quenching (Vj) and reduced electron transport (REo/RC),

suggests energy diversion from photosynthetic machinery maintenance to growth processes. This strategy, while supporting short-term growth, may compromise long-term stress adaptation by depleting energy reserves needed for ion homeostasis. This trade-off may relate to its parentage ((*V. berlandieri* × *V. riparia*) × (*V. vinifera* × *V. berlandieri*)) [83], as *V. riparia* is known for vigorous growth but moderate salt sensitivity.

M4 consistently showed the highest sensitivity to salinity stress across most parameters. It experienced the most severe reductions in biomass, exhibited poor growth maintenance, and showed accelerated progression of stress symptoms. These results contrast with previous findings by Meggio et al. [24], who reported better performance under water and salinity stress.

1103 Paulsen displayed moderate but stable responses across most parameters. While showing intermediate growth reduction, it maintained superior photosynthetic efficiency and demonstrated effective photoprotective mechanisms under stress, confirming previous reports of its salt tolerance [59]. This stability reflects a distinct physiological strategy: unlike M2's growth-focused approach, 1103 Paulsen invests significant energy in maintaining photosynthetic machinery and ion compartmentalization, particularly in vacuoles. This strategy ensures sustained photoassimilate production under stress while effectively managing ion balance [62]. Its unique mid-experiment increase in SPAD values suggests sophisticated stress adaptation capabilities, particularly in maintaining photosynthetic apparatus functionality.

R110 exhibited contrasting performance across different parameters. While maintaining relatively stable biomass under moderate stress and showing effective chloride exclusion, it demonstrated a severe reduction in shoot length under high salinity. Its maintenance of higher K^+/Na^+ and Ca^{2+}/Na^+ ratios under control conditions, followed by pronounced decreases under stress, suggests initially effective but ultimately limited ion homeostasis mechanisms.

The relative performance of rootstocks varied significantly depending on the parameter evaluated. While M2 demonstrated the highest overall salt tolerance, followed by 1103 Paulsen, R110, and M4, this general ranking masks important parameter-specific variations. When examining photosynthetic efficiency, 1103 Paulsen exhibited the best performance, followed by R110, with M2 showing moderate efficiency and M4 displaying the lowest values. Growth parameters revealed a different pattern, with M2 maintaining the best performance, followed by R110 and 1103 Paulsen, and M4 again showing the poorest response. In terms of ion homeostasis, 1103 Paulsen demonstrated superior regulation, with M2 showing good capacity, followed by R110, while M4 exhibited the least effective ion management. These varying patterns highlight the complexity of salt tolerance mechanisms and the importance of considering multiple parameters when evaluating rootstock performance.

4.7. Applicability of Findings, Study Limitations, and Future Research Directions

The comprehensive characterization of genotype-specific responses to salinity stress for these four rootstocks provides valuable insights for both practical viticulture and theoretical understanding of salt tolerance mechanisms in woody plants. For rootstock selection and breeding programs, the identified patterns of stress response provide valuable guidance. Under moderate salinity (25–50 mM NaCl), M2 is optimal where growth maintenance is crucial, while in high salinity areas (>50 mM NaCl), 1103 Paulsen offers the most stable overall performance. For regions with fluctuating salinity levels, R110's balanced ion regulation capacity may be advantageous. From a breeding perspective, several promising trait combinations emerge: M2's superior growth maintenance mechanisms could be combined with 1103 Paulsen's effective ion partitioning strategy to develop more resilient rootstocks.

Additionally, R110's efficient ion exclusion capacity, particularly for Cl^- and Na^+, represents a valuable trait for introgression. The parameter-specific variations observed suggest breeding efforts should target complementary trait combinations rather than overall salt tolerance. These identified traits and stress response patterns can guide the development of more salt-tolerant rootstocks.

For vineyard management, particularly in areas affected by brackish irrigation water and/or soil salinity, the reported characterization of genotype-specific thresholds and response patterns enables more informed rootstock selection. The clear identification of critical salinity thresholds (particularly around 50–75 mM NaCl) provides practical guidelines for irrigation management and soil salinity monitoring.

While our study focuses on genotype selection, managing vineyards under saline conditions requires an integrated approach (Figure 9). An effective management framework begins with a comprehensive soil health assessment involving analysis of physical, chemical, and biological properties. Particular attention must be paid to electrical conductivity (EC), pH, and sodium adsorption ratio (SAR) for identifying and monitoring salt-affected areas.

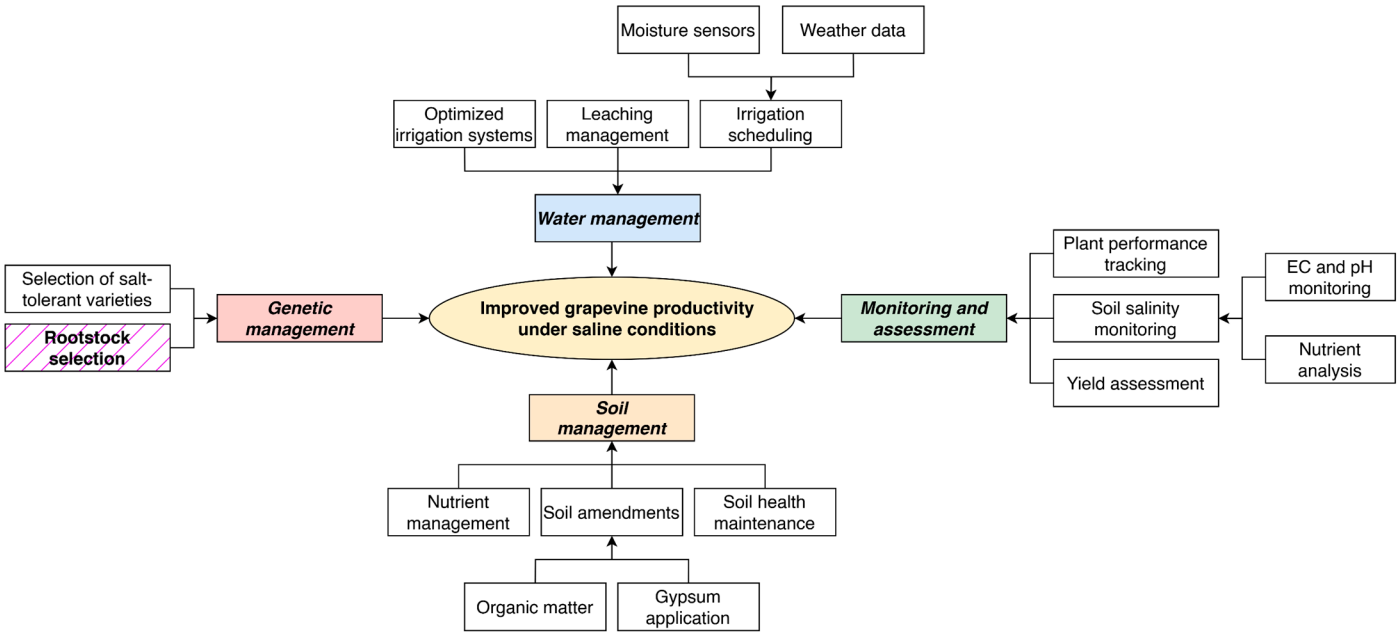

Figure 9. Management framework for grapevine cultivation under saline conditions.

Management strategies guided by soil assessment include several key interventions. Gypsum application improves soil structure and enhances salt leaching, while optimized irrigation methods through drip systems and appropriate leaching fractions ensure efficient water management. Incorporating organic matter boosts microbial activity and nutrient availability. Advanced monitoring tools like sensors and GIS technology enable continuous soil assessment, ensuring precise, timely adjustments to these interventions. This holistic approach allows growers to maximize the benefits of salt-tolerant genotypes while maintaining soil health and ensuring long-term vineyard sustainability.

The observed organ-specific responses and ion distribution patterns offer insights useful for cultural practices. Understanding how different rootstocks manage ion distribution can inform nutrient management approaches in saline conditions. The differential responses in ion accumulation patterns also suggest possibilities for optimizing fertilization practices based on rootstock-specific characteristics.

Concerning study limitations, several experimental constraints should be considered when interpreting the presented results. The controlled greenhouse environment, while

allowing precise stress manipulation, limits the direct field application of our findings. Future research should expand to include multi-site field trials across different soil types, evaluate varying irrigation water qualities with different SAR values (from 0 to 15), and integrate these factors with different deficit irrigation strategies under field conditions.

The temporal scope of our study presents another significant limitation. The five-month experimental duration, though sufficient for observing acute stress responses, may not fully capture the long-term adaptation mechanisms that grapevines develop over multiple growing seasons. We recommend conducting field trials with a minimum duration of three years to assess seasonal variations in response patterns and evaluate performance across multiple growing cycles.

Methodological constraints also warrant consideration. The irrigation management strategy—maintaining soil moisture at field capacity with a 20–30% leaching fraction—differs from typical vineyard conditions. Our focus on NaCl as a single salt source, while providing clear experimental control, does not fully represent the complexity of field conditions. Future studies should incorporate mixed salt compositions including various ionic combinations (Na^+, Cl^-, Ca^{2+}, Mg^{2+}, SO_4^{2-}, HCO_3^-), evaluate interactions between salinity and water stress, and assess how different rootstock–scion combinations respond to these complex stress conditions.

The immediate research priorities, spanning the next one to two years, should focus on field validation trials in commercial vineyards to verify our greenhouse findings. These studies should include economic impact assessments of different rootstock choices and develop rapid screening protocols for salt tolerance evaluation. Medium-term research objectives, projected over two to five years, should examine rootstock–scion interactions under saline conditions, investigate molecular markers associated with salt tolerance mechanisms, and develop site-specific management protocols based on local conditions and constraints. Long-term research goals, extending beyond five years, should address climate change adaptation strategies in viticulture, provide recommendations for breeding programs based on accumulated field data, and develop regional rootstock selection models that integrate multiple stress factors.

These findings also contribute to climate change adaptation strategies in viticulture, as soil and water salinization becomes increasingly prevalent. The identified differences in stress response mechanisms can inform the development of region-specific rootstock recommendations based on projected salinity challenges.

5. Conclusions

This study underscores the complexity of salinity stress responses in grapevine rootstocks, highlighting distinct genotype-specific adaptations. While no single rootstock excelled universally, M2 exhibited strong growth resilience under salinity stress, though with vulnerabilities in ion homeostasis. 1103 Paulsen showed a balanced response, maintaining photosynthetic efficiency and effective adaptation mechanisms, whereas R110 demonstrated efficient ion regulation under moderate stress but struggled at higher salinity levels. M4 displayed limited overall adaptability to saline conditions. A critical salinity threshold between 50 and 75 mM NaCl was identified, beyond which stress responses shifted from adaptive to damaging. Organ-specific ion distribution patterns revealed genotype-dependent regulatory mechanisms, particularly in Na^+, Cl^-, K^+, and Ca^{2+} management. These findings have practical implications for viticulture, particularly in regions facing soil salinization. The detailed characterization of rootstocks provides valuable insights for targeted breeding and selection strategies. Future research should investigate molecular mechanisms underlying M2's growth resilience and 1103 Paulsen's photosyn-

thetic stability, complemented by field trials to validate these findings under diverse environmental conditions.

Supplementary Materials: The following supporting information can be downloaded at: https://www.mdpi.com/article/10.3390/agronomy15020473/s1, Figure S1: Error bar graph for fresh weight as a function of the rootstock genotype × treatment interaction; Figure S2: Error bar graph for fresh weight as a function of the organ × treatment interaction; Figure S3: Error bar graph for dry weight as a function of the rootstock genotype × treatment interaction; Figure S4: Error bar graph for dry weight as a function of the organ × treatment interaction; Figure S5: Spline representation of shoot lengths for each rootstock genotype as a function of treatment and date; Figure S6: Spline representation of trunk diameters for each rootstock genotype as a function of treatment and date; Figure S7: (a) Efficiency of photosystem II, (b) energy and electron transport, (c) energy dissipation; Figure S8: Splines for stomatal conductance (mmol H_2O m^{-2} s^{-1}) for genotypes by treatment and date; Figure S9: Spline representation of SPAD for each rootstock genotype as a function of treatment and date; Figure S10: Error bar graph for Ca^{2+} content as a function of the rootstock genotype × treatment interaction; Figure S11: Error bar graph for Ca^{2+} content as a function of the organ × treatment interaction; Figure S12: Error bar graph for K^+ content as a function of the rootstock genotype × treatment interaction; Figure S13: Error bar graph for K^+ content as a function of the organ × treatment interaction; Figure S14: Error bar graph for Cl^- content as a function of the rootstock genotype × treatment interaction; Figure S15: Error bar graph for Cl^- content as a function of the organ × treatment interaction; Figure S16: Error bar graph for Na^+ content as a function of the rootstock genotype × treatment interaction; Figure S17: Error bar graph for Na^+ content as a function of the organ × treatment interaction; Figure S18: Error bar graph for K^+/Na^+ ratio as a function of the rootstock genotype × treatment interaction; Figure S19: Error bar graph for K^+/Na^+ ratio as a function of the organ × treatment interaction; Figure S20: Error bar graph for Ca^{2+}/Na^+ ratio as a function of the rootstock genotype × treatment interaction; Figure S21: Error bar graph for Ca^{2+}/Na^+ ratio as a function of the organ × treatment interaction; Table S1: Statistical data for fresh weight as a function of the rootstock genotype × treatment interaction; Table S2: Statistical data for fresh weight as a function of the treatment × organ interaction; Table S3: Statistical data for dry weight as a function of the rootstock genotype × treatment interaction; Table S4: Statistical data for dry weight as a function of the treatment × organ interaction; Table S5: Spline data for the effects of rootstock genotype and treatment combinations on shoot length; Table S6: Spline data for the effects of rootstock genotype and treatment combinations on trunk diameter; Table S7: Descriptive statistics of fluorimeter measurements; Table S8: Spline data for the effects of rootstock genotype and treatment combinations on stomatal conductance; Table S9: Spline data for the effects of rootstock genotype and treatment combinations on SPAD values; Table S10: Temporal evolution of salinity-induced leaf damage in different grapevine rootstock genotypes under 50 mM (S3) and 75 mM (S4) NaCl treatments; Table S11: Statistical data for the factorial models log(variable); Table S12: Robust comparisons of the group *p*-values of each of the factors along with their interactions; Table S13: Statistical data for Ca^{2+} content as a function of the rootstock genotype × treatment interaction; Table S14: Statistical data for Ca^{2+} content as a function of the treatment × organ interaction; Table S15: Statistical data for K^+ content as a function of the rootstock genotype × treatment interaction; Table S16: Statistical data for K^+ content as a function of the treatment × organ interaction; Table S17: Statistical data for Cl^- content as a function of the rootstock genotype × treatment interaction; Table S18: Statistical data for Cl^- content as a function of the treatment × organ interaction; Table S19: Statistical data for Na^+ content as a function of the rootstock genotype × treatment interaction; Table S20: Statistical data for Na^+ content as a function of the treatment × organ interaction; Table S21: Statistical data for K^+/Na^+ ratio as a function of the rootstock genotype × treatment interaction; Table S22: Statistical data for K^+/Na^+ ratio as a function of the treatment × organ interaction; Table S23: Statistical data for Ca^{2+}/Na^+ ratio as a function of the rootstock genotype × treatment interaction; Table S24: Statistical data for Ca^{2+}/Na^+ ratio as a function of the treatment × organ interaction.

Author Contributions: Conceptualization, X.R.-G., J.C.-G. and P.M.-R.; methodology, M.V.-M., J.C.-G., L.A.-R. and P.M.-R.; software, L.A.-R.; validation, J.C.-G.; formal analysis, X.R.-G., M.V.-M., J.C.-G., L.A.-R. and P.M.-R.; investigation, X.R.-G., M.V.-M., J.C.-G. and P.M.-R.; resources, X.R.-G.; data curation, L.A.-R.; writing—original draft preparation, X.R.-G., M.V.-M., J.C.-G., L.A.-R. and P.M.-R.; writing—review and editing, X.R.-G. and P.M.-R.; visualization, X.R.-G., J.C.-G. and L.A.-R.; supervision, M.V.-M. and J.C.-G. All authors have read and agreed to the published version of the manuscript.

Funding: This research received no external funding.

Data Availability Statement: All data supporting the findings of this study are available within the paper and its Supplementary Information. Should any raw data files be needed in another format, they are available from the corresponding author upon reasonable request.

Conflicts of Interest: Author Xavier Rius-Garcia was employed by the company Agromillora Group. All authors declare that the research was conducted in the absence of any commercial or financial relationships that could be construed as a potential conflict of interest.

Abbreviations

The following abbreviations are used in this manuscript:

Area	Area above the fluorescence induction curve between the F_0 and F_m. Related to the pool size of electron acceptors in the photo-synthetic electron transport chain
DIo/CSo	Energy dissipated in the form of heat and fluorescence per cross-section.
DIo/RC	Energy dissipated in the form of heat and fluorescence per reaction center.
EC	Electrical conductivity.
ETo/RC	Electron transport rate per reaction center.
F_0	Initial fluorescence.
F_m	Maximum fluorescence.
F_v	Variable fluorescence.
F_v/F_m	Maximum PSII quantum efficiency when all reaction centers are open.
N	QA turnover number, i.e., the number of times QA is reduced and oxidized during the measurement.
OJIP	Chlorophyll fluorescence transient phases O, J, I, and P.
PI(abs)	Performance index on absorption basis.
PSII	Photosystem II.
pXRF	Portable X-ray fluorescence.
QA	Primary quinone electron acceptor.
REo/RC	Electron transport rate per reaction center, i.e., the rate of electron transport beyond QA per reaction center.
ROS	Reactive oxygen species.
SAR	Sodium adsorption ratio.
Sm	Normalized total complementary area above the OJIP transient. Related to the energy needed to close all PSII reaction centers.
Vj	Relative variable fluorescence at the J-step of the OJIP fluorescence transient. Provides information about the reduction state of the primary quinone electron acceptor.
φ(Po)	Maximum quantum yield of primary photochemistry.
ψ(Eo)	Efficiency with which a trapped exciton can move an electron into the electron transport chain beyond QA.

References

1. Nikolaou, K.-E.; Chatzistathis, T.; Theocharis, S.; Argiriou, A.; Koundouras, S.; Zioziou, E. Effects of salinity and rootstock on nutrient element concentrations and physiology in own-rooted or grafted to 1103 P and 101-14 Mgt rootstocks of Merlot and Cabernet Franc grapevine cultivars under climate change. *Sustainability* **2021**, *13*, 2477. [CrossRef]
2. OIV. *State of the World Vine and Wine Sector in 2023*; International Organisation of Vine and Wine: Dijon, France, 2024; p. 21.

3. Cramer, G.R. Abiotic stress and plant responses from the whole vine to the genes. *Aust. J. Grape Wine Res.* **2010**, *16*, 86–93. [CrossRef]
4. Schultz, H.R.; Stoll, M. Some critical issues in environmental physiology of grapevines: Future challenges and current limitations. *Aust. J. Grape Wine Res.* **2010**, *16*, 4–24. [CrossRef]
5. Jones, G.V.; White, M.A.; Cooper, O.R.; Storchmann, K. Climate change and global wine quality. *Clim. Change* **2005**, *73*, 319–343. [CrossRef]
6. Prada, J.; Dinis, L.-T.; Soriato, E.; Vandelle, E.; Soletkin, O.; Uysal, Ş.; Dihazi, A.; Santos, C.; Santos, J.A. Climate change impact on Mediterranean viticultural regions and site-specific climate risk-reduction strategies. *Mitig. Adapt. Strateg. Glob. Change* **2024**, *29*, 52. [CrossRef]
7. Prior, L.D.; Grieve, A.M.; Cullis, B.R. Sodium chloride and soil texture interactions in irrigated field grown sultana grapevines. I. Yield and fruit quality. *Aust. J. Agric. Res.* **1992**, *43*, 1051. [CrossRef]
8. Stevens, R.M.; Harvey, G.; Partington, D.L. Irrigation of grapevines with saline water at different growth stages: Effects on leaf, wood and juice composition. *Aust. J. Grape Wine Res.* **2011**, *17*, 239–248. [CrossRef]
9. da Silva, E.F.; Santos, H.R.B.; Ometto, J.P.H.B.; Jardim, A.M.d.R.F.; Silva, T.G.F.d.; Hermínio, P.J.; Simões, A.N.; Souza, E.; Ferreira-Silva, S.L. Salt-excluder rootstock improves physio-biochemical responses of grafted grapevine plants subjected to salinity stress. *Curr. Plant Biol.* **2024**, *37*, 100316. [CrossRef]
10. Cataldo, E.; Fucile, M.; Manzi, D.; Peruzzi, E.; Mattii, G.B. Effects of Zeowine and compost on leaf functionality and berry composition in Sangiovese grapevines. *J. Agric. Sci.* **2023**, *161*, 412–427. [CrossRef]
11. Cataldo, E.; Puccioni, S.; Eichmeier, A.; Natale, R.; Gori, M.; Biricolti, S.; Mattii, G.B. Effect of zeolite and irrigation treatments on grapevine leaves, an interdisciplinary approach. *Plant Soil* **2024**. [CrossRef]
12. Sabir, A.; Gayretli, Y.; Abdulhadi, S.A.A.; Karaca, U.C. Differential responses of grapevine rootstocks (*Vitis* spp.) to saline irrigation water applications. *Erwerbs-Obstbau* **2021**, *63*, 9–14. [CrossRef]
13. Walker, R.R.; Blackmore, D.H.; Dunlevy, J.D.; Edwards, E.J.; Walker, A.R. Rootstock type influences salt exclusion response of grafted Shiraz under salt treatment at elevated root zone temperature. *Aust. J. Grape Wine Res.* **2022**, *28*, 292–303. [CrossRef]
14. Gajjar, P.; Ismail, A.; Islam, T.; Darwish, A.G.; Moniruzzaman, M.; Abuslima, E.; Dawood, A.S.; El-Saady, A.M.; Tsolova, V.; El-Kereamy, A.; et al. Physiological comparison of two salt-excluder hybrid grapevine rootstocks under salinity reveals different adaptation qualities. *Plants* **2023**, *12*, 3247. [CrossRef]
15. Zhou-Tsang, A.; Wu, Y.; Henderson, S.W.; Walker, A.R.; Borneman, A.R.; Walker, R.R.; Gilliham, M. Grapevine salt tolerance. *Aust. J. Grape Wine Res.* **2021**, *27*, 149–168. [CrossRef]
16. Storey, R.; Schachtman, D.P.; Thomas, M.R. Root structure and cellular chloride, sodium and potassium distribution in salinized grapevines. *Plant Cell Environ.* **2003**, *26*, 789–800. [CrossRef]
17. Fisarakis, I.; Chartzoulakis, K.; Stavrakas, D. Response of Sultana vines (*V. vinifera* L.) on six rootstocks to NaCl salinity exposure and recovery. *Agric. Water Manag.* **2001**, *51*, 13–27. [CrossRef]
18. Vila, H.F.; Di Filippo, M.L.; Venier, M.; Filippini, M.F. How rootstocks influence salt tolerance in grapevine? The roles of conferred vigor and ionic exclusion. *Acta Hortic.* **2016**, *1136*, 145–154. [CrossRef]
19. Ollat, N.; Peccoux, A.; Papura, D.; Esmenjaud, D.; Marguerit, E.; Tandonnet, J.P.; Bordenave, L.; Cookson, S.J.; Barrieu, F.; Rossdeutsch, L.; et al. Rootstocks as a component of adaptation to environment. In *Grapevine in a Changing Environment: A Molecular and Ecophysiological Perspective*; Gerós, H., Chaves, M.M., Medrano Gil, H., Delrot, S., Eds.; John Wiley & Sons: Chichester, UK, 2015; pp. 68–108. [CrossRef]
20. Keller, M. *The Science of Grapevines: Anatomy and Physiology*, 2nd ed.; Elsevier/Academic Press: Amsterdam, The Netherlands; Boston, MA, USA, 2015; p. 509.
21. Quénol, H.; Marie, G.; Barbeau, G.; Van Leeuwen, C.; Hofmann, M.; Foss, C.; Irimia, L.; Rochard, J.; Boulanger, J.-P.; Tissot, C. Adaptation of viticulture to climate change: High resolution observations of adaptation scenario for viticulture: The ADVICLIM European project. *Bull. De L'oiv* **2014**, *87*, 395–406.
22. Bianchi, D.; Brancadoro, L. Water use efficiency and nutritional status of a new grapevine rootstock selection. *Horticulturae* **2021**, *7*, 503. [CrossRef]
23. Bianchi, D.; Grossi, D.; Tincani, D.T.G.; Simone Di Lorenzo, G.; Brancadoro, L.; Rustioni, L. Multi-parameter characterization of water stress tolerance in *Vitis* hybrids for new rootstock selection. *Plant Physiol. Biochem.* **2018**, *132*, 333–340. [CrossRef]
24. Meggio, F.; Prinsi, B.; Negri, A.S.; Simone Di Lorenzo, G.; Lucchini, G.; Pitacco, A.; Failla, O.; Scienza, A.; Cocucci, M.; Espen, L. Biochemical and physiological responses of two grapevine rootstock genotypes to drought and salt treatments. *Aust. J. Grape Wine Res.* **2014**, *20*, 310–323. [CrossRef]
25. Porro, D.; Pedò, S.; Bertoldi, D.; Bortolotti, L.; Failla, O.; Zamboni, M. Evaluation of new rootstocks for grapevine: Nutritional aspects. *Acta Hortic.* **2013**, *984*, 109–115. [CrossRef]
26. Hoagland, D.R.; Arnon, D.I. *The Water-Culture Method for Growing Plants Without Soil*; College of Agriculture, University of California; California Agricultural Experiment Station: Berkeley, CA, USA, 1950; p. 31.

27. Perica, S.; Goreta, S.; Selak, G.V. Growth, biomass allocation and leaf ion concentration of seven olive (*Olea europaea* L.) cultivars under increased salinity. *Sci. Hortic.* **2008**, *117*, 123–129. [CrossRef]
28. Sapkota, Y.; McDonald, L.M.; Griggs, T.C.; Basden, T.J.; Drake, B.L. Portable x-ray fluorescence spectroscopy for rapid and cost-effective determination of elemental composition of ground forage. *Front. Plant Sci.* **2019**, *10*, 317. [CrossRef]
29. Antonangelo, J.; Zhang, H. Soil and plant nutrient analysis with a portable XRF probe using a single calibration. *Agronomy* **2021**, *11*, 2118. [CrossRef]
30. Towett, E.K.; Shepherd, K.D.; Lee Drake, B. Plant elemental composition and portable X-ray fluorescence (pXRF) spectroscopy: Quantification under different analytical parameters. *X-Ray Spectrom.* **2016**, *45*, 117–124. [CrossRef]
31. McGladdery, C.; Weindorf, D.C.; Chakraborty, S.; Li, B.; Paulette, L.; Podar, D.; Pearson, D.; Kusi, N.Y.O.; Duda, B. Elemental assessment of vegetation via portable X-ray fluorescence (pXRF) spectrometry. *J. Environ. Manag.* **2018**, *210*, 210–225. [CrossRef] [PubMed]
32. Singh, V.K.; Sharma, N.; Singh, V.K. Application of X-ray fluorescence spectrometry in plant science: Solutions, threats, and opportunities. *X-Ray Spectrom.* **2021**, *51*, 304–327. [CrossRef]
33. Jones, J.B.; Case, V.W. Sampling, handling, and analyzing plant tissue samples. In *Soil Testing and Plant Analysis*, 3rd ed.; Westerman, R.L., Ed.; Soil Science Society of America: Madison, WI, USA, 2018; Volume 3, pp. 389–427.
34. Kalra, Y. *Handbook of Reference Methods for Plant Analysis*; CRC Press: Boca Raton, FL, USA, 1997; p. 320. [CrossRef]
35. Kalaji, H.M.; Schansker, G.; Ladle, R.J.; Goltsev, V.; Bosa, K.; Allakhverdiev, S.I.; Brestic, M.; Bussotti, F.; Calatayud, A.; Dąbrowski, P.; et al. Frequently asked questions about in vivo chlorophyll fluorescence: Practical issues. *Photosynth. Res.* **2014**, *122*, 121–158. [CrossRef] [PubMed]
36. Stirbet, A.; Govindjee. On the relation between the Kautsky effect (chlorophyll a fluorescence induction) and Photosystem II: Basics and applications of the OJIP fluorescence transient. *J. Photochem. Photobiol. B* **2011**, *104*, 236–257. [CrossRef]
37. Strasser, R.J.; Tsimilli-Michael, M.; Srivastava, A. Analysis of the chlorophyll *a* fluorescence transient. In *Chlorophyll a Fluorescence: A Signature of Photosynthesis*; Papageorgiou, G.C., Govindjee, Eds.; Springer: Dordrecht, The Netherlands, 2004; pp. 321–362. [CrossRef]
38. Boussadia, O.; Steppe, K.; Zgallai, H.; El Hadj, S.B.; Braham, M.; Lemeur, R.; Van Labeke, M.C. Nondestructive determination of nitrogen and chlorophyll content in olive tree leaves and the relation with photosynthesis and fluorescence parameters. *Photosynthetica* **2011**, *49*, 149–153. [CrossRef]
39. R Core Team. *R: A Language and Environment for Statistical Computing*; R Foundation for Statistical Computing: Vienna, Austria, 2021.
40. Lilliefors, H.W. On the Kolmogorov-Smirnov test for normality with mean and variance unknown. *J. Am. Stat. Assoc.* **1967**, *62*, 399–402. [CrossRef]
41. Shapiro, S.S.; Wilk, M.B. An analysis of variance test for normality (complete samples). *Biometrika* **1965**, *52*, 591–611. [CrossRef]
42. Brown, M.B.; Forsythe, A.B. Robust tests for the equality of variances. *J. Am. Stat. Assoc.* **1974**, *69*, 364. [CrossRef]
43. Kruskal, W.H.; Wallis, W.A. Use of ranks in one-criterion variance analysis. *J. Am. Stat. Assoc.* **1952**, *47*, 583–621. [CrossRef]
44. Wilcox, R.R. *Introduction to Robust Estimation and Hypothesis Testing*, 5th ed.; Academic Press: London, UK, 2021.
45. Welch, B.L. On the comparison of several mean values: An alternative approach. *Biometrika* **1951**, *38*, 330–336. [CrossRef]
46. Mond, C.E.D.; Lenth, R.V. A robust confidence interval for location. *Technometrics* **1987**, *29*, 211. [CrossRef]
47. Harrell, F.E. *Regression Modeling Strategies. With Applications to Linear Models, Logistic and Ordinal Regression, and Survival Analysis*, 2nd ed.; Springer Cham: New York, NY, USA, 2015; p. 582. [CrossRef]
48. Friedman, J.H. Multivariate adaptive regression splines. *Ann. Stat.* **1991**, *19*. [CrossRef]
49. Durrleman, S.; Simon, R. Flexible regression models with cubic splines. *Stat. Med.* **2006**, *8*, 551–561. [CrossRef] [PubMed]
50. Krzanowski, W.J. *An Introduction to Statistical Modelling*; Wiley: London, UK, 2010; p. 272.
51. Akaike, H. Information theory and an extension of the maximum likelihood principle. In *Selected Papers of Hirotugu Akaike*; Parzen, E., Tanabe, K., Kitagawa, G., Eds.; Springer: New York, NY, USA, 1998; pp. 199–213. [CrossRef]
52. Schwarz, G. Estimating the dimension of a model. *Ann. Stat.* **1978**, *6*, 461–464. [CrossRef]
53. Chen, J.; Chen, Z. Extended Bayesian information criteria for model selection with large model spaces. *Biometrika* **2008**, *95*, 759–771. [CrossRef]
54. Munns, R.; Tester, M. Mechanisms of salinity tolerance. *Annu. Rev. Plant Biol.* **2008**, *59*, 651–681. [CrossRef] [PubMed]
55. Acosta-Motos, J.; Ortuño, M.; Bernal-Vicente, A.; Diaz-Vivancos, P.; Sanchez-Blanco, M.; Hernandez, J. Plant responses to salt stress: Adaptive mechanisms. *Agronomy* **2017**, *7*, 18. [CrossRef]
56. Shani, U.; Ben-Gal, A. Long-term response of grapevines to salinity: Osmotic effects and ion toxicity. *Am. J. Enol. Vitic.* **2005**, *56*, 148. [CrossRef]
57. Martin, L.; Vila, H.; Bottini, R.; Berli, F. Rootstocks increase grapevine tolerance to NaCl through ion compartmentalization and exclusion. *Acta Physiol. Plant* **2020**, *42*, 145. [CrossRef]
58. Chaves, M.M.; Flexas, J.; Pinheiro, C. Photosynthesis under drought and salt stress: Regulation mechanisms from whole plant to cell. *Ann. Bot.* **2009**, *103*, 551–560. [CrossRef] [PubMed]

59. Walker, R.R.; Blackmore, D.H.; Clingeleffer, P.R.; Emanuelli, D. Rootstock type determines tolerance of Chardonnay and Shiraz to long-term saline irrigation. *Aust. J. Grape Wine Res.* **2014**, *20*, 496–506. [CrossRef]
60. Parida, A.K.; Das, A.B. Salt tolerance and salinity effects on plants: A review. *Ecotoxicol. Environ. Saf.* **2005**, *60*, 324–349. [CrossRef] [PubMed]
61. Saritha, K.; Vijaya, D.; Srinivas Rao, B.; Padma, M. Relative salt tolerance of different grape rootstocks to NaCl. *Int. J. Curr. Microbiol. Appl. Sci.* **2016**, *5*, 723–733. [CrossRef]
62. Lo'ay, A.A.; El-Ezz, S.F.A. Performance of 'Flame seedless' grapevines grown on different rootstocks in response to soil salinity stress. *Sci. Hortic.* **2021**, *275*, 109704. [CrossRef]
63. Flexas, J.; Barbour, M.M.; Brendel, O.; Cabrera, H.M.; Carriquí, M.; Díaz-Espejo, A.; Douthe, C.; Dreyer, E.; Ferrio, J.P.; Gago, J.; et al. Mesophyll diffusion conductance to CO_2: An unappreciated central player in photosynthesis. *Plant Sci.* **2012**, *193–194*, 70–84. [CrossRef] [PubMed]
64. Murchie, E.H.; Lawson, T. Chlorophyll fluorescence analysis: A guide to good practice and understanding some new applications. *J. Exp. Bot.* **2013**, *64*, 3983–3998. [CrossRef]
65. Ashraf, M.; Harris, P.J.C. Photosynthesis under stressful environments: An overview. *Photosynthetica* **2013**, *51*, 163–190. [CrossRef]
66. Askri, H.; Gharbi, F.; Rejeb, S.; Mliki, A.; Ghorbel, A. Differential physiological responses of Tunisian wild grapevines (*Vitis vinifera* L. subsp. *sylvestris*) to NaCl salt stress. *Braz. J. Bot.* **2018**, *41*, 795–804. [CrossRef]
67. Foyer, C.H.; Shigeoka, S. Understanding oxidative stress and antioxidant functions to enhance photosynthesis. *Plant Physiol.* **2011**, *155*, 93–100. [CrossRef]
68. El-Salhy, A.M.; Mostafa, R.A.A.; Ahmed-Roqia, B.; Ali, H.A.M. Responses of some grapevine rootstocks to long-term salinity and drought stress conditions. *Middle East J. Agric. Res.* **2014**, *3*, 479–490.
69. Lupo, Y.; Schlisser, A.; Dong, S.; Rachmilevitch, S.; Fait, A.; Lazarovitch, N. Root system response to salt stress in grapevines (*Vitis* spp.): A link between root structure and salt exclusion. *Plant Sci.* **2022**, *325*, 111460. [CrossRef] [PubMed]
70. Zhang, X.; Walker, R.R.; Stevens, R.M.; Prior, L.D. Yield-salinity relationships of different grapevine (*Vitis vinifera* L.) scion-rootstock combinations. *Aust. J. Grape Wine Res.* **2002**, *8*, 150–156. [CrossRef]
71. Mansour, M.M.F. Role of vacuolar membrane transport systems in plant salinity tolerance. *J. Plant Growth Regul.* **2022**, *42*, 1364–1401. [CrossRef]
72. Shabala, S.; Cuin, T.A. Potassium transport and plant salt tolerance. *Physiol. Plant.* **2008**, *133*, 651–669. [CrossRef]
73. Rengel, Z. The role of calcium in salt toxicity. *Plant Cell Environ.* **1992**, *15*, 625–632. [CrossRef]
74. Khan, M.M.; Akram, M.T.; Qadri, R.W.K.; Al-Yahyai, R. Role of grapevine rootstocks in mitigating environmental stresses: A review. *J. Agric. Mar. Sci.* **2020**, *25*, 1–12. [CrossRef]
75. Shabala, S.; Pottosin, I. Regulation of potassium transport in plants under hostile conditions: Implications for abiotic and biotic stress tolerance. *Physiol. Plant.* **2014**, *151*, 257–279. [CrossRef] [PubMed]
76. Läuchli, A.; Grattan, S.R. Plant growth and development under salinity stress. In *Advances in Molecular Breeding Toward Drought and Salt Tolerant Crops*; Jenks, M.A., Hasegawa, P.M., Jain, S.M., Eds.; Springer: Dordrecht, The Netherlands, 2007; pp. 1–32. [CrossRef]
77. Tregeagle, J.M.; Tisdall, J.M.; Blackmore, D.H.; Walker, R.R. A diminished capacity for chloride exclusion by grapevine rootstocks following long-term saline irrigation in an inland versus a coastal region of Australia. *Aust. J. Grape Wine Res.* **2006**, *12*, 178–191. [CrossRef]
78. Zhang, J.-L.; Flowers, T.J.; Wang, S.-M. Mechanisms of sodium uptake by roots of higher plants. *Plant Soil* **2009**, *326*, 45–60. [CrossRef]
79. Flowers, T.J.; Munns, R.; Colmer, T.D. Sodium chloride toxicity and the cellular basis of salt tolerance in halophytes. *Ann. Bot.* **2015**, *115*, 419–431. [CrossRef] [PubMed]
80. Zhao, B.; Liu, Z.; Zhu, C.; Zhang, Z.; Shi, W.; Lu, Q.; Sun, J. Saline–alkaline stress resistance of Cabernet Sauvignon grapes grafted on different rootstocks and rootstock combinations. *Plants* **2023**, *12*, 2881. [CrossRef]
81. Sivritepe, N.; Sivritepe, H.O.; Celik, H.; Katkat, A.V. Salinity responses of grafted grapevines: Effects of scion and rootstock genotypes. *Not. Bot. Horti Agrobot. Cluj-Napoca* **2010**, *38*, 193–201. [CrossRef]
82. Hasegawa, P.M.; Bressan, R.A.; Zhu, J.-K.; Bohnert, H.J. Plant cellular and molecular responses to high salinity. *Annu. Rev. Plant Physiol. Plant Mol. Biol.* **2000**, *51*, 463–499. [CrossRef]
83. Chen, Y.; Fei, Y.; Howell, K.; Chen, D.; Clingeleffer, P.; Zhang, P. Rootstocks for grapevines now and into the future: Selection of rootstocks based on drought tolerance, soil nutrient availability, and soil pH. *Aust. J. Grape Wine Res.* **2024**, *2024*, 6704238. [CrossRef]